ABSTRACT

Title of Document:	OXYGEN MEASUREMENT DURING CELL CULTURE: FROM MULTIWELL-PLATES TO MICROFLUIDIC DEVICES
	Peter Chung Thomas, Doctor of Philosophy 2011
Directed By:	Professor Srinivasa R. Raghavan, Department of Chemical and Biomolecular Engineering

Oxygen is an important regulator of normal cell behavior. Proper supply of oxygen is required to maintain ATP production, while perturbation of oxygen supply alters cell behavior and leads to tissue damage and cell death. *In vivo,* cells are exposed to a mean partial pressure of oxygen between 0.03 to 0.09 atm that is tissue specific. In contrast, conventional cell cultures are routinely performed at an atmospheric oxygen level of 0.21 atm. The disparity between *in vivo* and *in vitro* oxygen levels have been shown to affect cell viability, growth and differentiation. Continuous measurements and control of oxygen levels are thus critical to maintaining proper cell behavior.

Current methods of oxygen measurement are invasive, difficult to integrate with microscopy and lack imaging capabilities. To improve the current state of measurements, we have developed a new non-invasive oxygen sensor for *in vitro* cell culture. The sensor was prepared by incorporating a porphyrin dye, Pt(II) meso-Tetra(pentafluoro-phenyl)porphine (PtTFPP), into gas permeable poly(dimethylsiloxane) (PDMS) thin films. The response of the sensor to oxygen followed the linear Stern-Volmer equation and demonstrated an order of magnitude higher sensitivity compared to other sensors (K_{SV} = 548 ± 71 atm^{-1}). A multilayer design created by sandwiching the PtTFPP-PDMS with a thin film of Teflon AF followed by a second layer of PDMS effectively mitigated against cytotoxicity effects and provided a suitable substrate for cell attachment. To demonstrate the utility of the sensor, oxygen measurements were made continuously with NIH 3T3 mouse fibroblast cells. The oxygen levels were found to decrease as a result of oxygen consumption by the cells. Using Fick's law, the data was analyzed and a per-cell oxygen consumption rate for the 3T3 fibroblasts was calculated. In addition, cells were clearly visualized on the sensor demonstrating the ability to integrate with phase-contrast and fluorescence microscopy.

Next, human hepatocellular carcinoma HepG2 were cultured on the oxygen sensor and continuous oxygen measurements showed a drastic decrease in oxygen level such that the cells were exposed to hypoxic conditions within 24 h. The per-cell oxygen consumption rate for HepG2 was determined to be 30 times higher than the 3T3 fibroblasts, confirming the high metabolic nature of these cells. At high densities, oxygen flux measurements showed an asymptotic behavior reaching the theoretical maximum of the culture condition. When the oxygen diffusion barrier was reduced, the oxygen flux increased, demonstrating insufficient

oxygenation for HepG2 at these densities. In routine culture, HepG2 adhere to their neighboring cells which results in formation of cell clusters. Oxygen measurement confirmed the presence of oxygen gradient across the cell clusters with the lowest oxygen levels observed in the middle.

Finally, we successfully integrated the oxygen sensor into microfluidic systems. The sensor provided real-time non-invasive measurements of oxygen levels on-chip. To regulate the oxygen levels in the device, water with different dissolved oxygen concentrations was used instead of gas. This method successfully mitigated the problems of pervaporation associated with previous devices. Physiologically relevant oxygen levels and oxygen gradients were easily generated on the device and the results showed excellent agreement with numerical simulations.

OXYGEN MEASUREMENT DURING CELL CULTURE: FROM MULTIWELL PLATES TO MICROFLUIDIC DEVICES

By

Peter C. Thomas

Dissertation submitted to the Faculty of the Graduate School of the
University of Maryland, College Park, in partial fulfillment
of the requirements for the degree of
Doctor of Philosophy
2011

Advisory Committee:
Prof. Srinivasa R. Raghavan, Dept. of Chemical and Biomolecular Engineering, Chair
Prof. Adam Hsieh, Dept. of Bioengineering
Prof. Ian White, Dept. of Bioengineering
Prof. Donald DeVoe, Dept. of Mechanical Engineering
Dr. Samuel P. Forry, National Institute of Standards and Technology

Dedication

I dedicate this work to my loving wife, Lan, my sister, Penny, and my parents, Emily and Lawrence. Without your support and encouragement I would not have been able to complete this journey. In addition, I also thank God for teaching me the valuable lessons of perseverance and determination through this work

Acknowledgements

I would like to thank my advisor at the University of Maryland, Professor Srinivasa Raghavan for his support and mentoring during my graduate school career. His dedication to his students is unmatched and I am grateful to have been one of his students.

I also want to give my sincerest gratitude to my advisor at the National Institute of Standards and Technology (NIST), Dr. Samuel P. Forry for his guidance and teaching over the years. I have grown so much as a scientist and I am thankful to have such an enriching learning experience working with him.

In addition, I want to thank Dr. Javier Atencia for the long conversations about life and science. They inspired me to always stay curious. I would also like to thank Dr. Laurie Locascio for giving me this very unique and wonderful opportunity to work at NIST, with whom all of this would not have been possible.

To all my friends at the University of Maryland and NIST, I am grateful to have met each one of you and it has been a pleasure to share and to discuss scientific ideas with you. And to my friends and family members, thank you for all your encouragements.

Table of Contents

Chapter 1

Introduction and Overview

1.1 Problem Description and Motivation

In vitro cell culture is a critical tool for how we understand biological systems, discover medicines and examine the fundamentals of diseases. Conventional cell culture techniques allow researchers to isolate cells of interests from tissue and grow them under controlled conditions outside of the body.[1,2] This provides a method to study basic cellular responses towards specific stimuli without the added complexity from an entire organism. The relevance of cell culture lies in its ability to generate physiologically relevant information without the need for animal studies. As such creating more biomimetic environments for cell culture is critical to ensuring proper cell responses that mimic the *in vivo* state.

For mammalian cells, one of the most critical parameters for survival is oxygen.[3] During aerobic respiration, oxygen is utilized as the electron acceptor at the end of the electron transport chain which then generates ATP.[4,5] This molecule is the key component that allows aerobic cells to generate high amounts of energy efficiently. Interesting, while many parameters have been examined in order to create the optimal conditions for cell growth, oxygen levels are routinely overlooked. Conventional cell cultures are usually performed under static atmospheric oxygen conditions with a partial pressure of oxygen (P_{O2}) equal to 0.21 atm with little regard to cell types. In contrast,

oxygen levels *in vivo* are much more dynamic and are finely tuned to meet the specific demands of different tissue and organs in the body.[6]

In vivo, oxygen levels are significantly lower than the atmospheric oxygen environment. Oxygen enters the body through the lungs and blood circulation transports oxygen to the different tissue in the body. In circulation the P_{O2} is approximately 0.12 atm while the mean tissue oxygen level is between 0.03 atm to 0.09 atm.[7] In other tissues such as the bone marrow or the kidney medullary, the P_{O2} is even lower between 0.01 atm to 0.03 atm.[8,9] This wide range of oxygen levels is the result of oxygen consumption by the surrounding cells as oxygen passes through different tissues via blood circulation.[7] Comparatively, the uniform oxygen level used in cell culture exhibits significant deviations from the oxygen environment *in vivo*, thus potentially changing cell behavior and confounding experimental results. For example, stem cells cultured under lower physiologic oxygen levels consistently show enhanced proliferation and reduced apoptosis compared to cells cultured at atmospheric oxygen conditions.[10] These reports highlight the need to monitor and control oxygen levels to preserve proper cell behaviors in order to generate experimental findings that are physiologically relevant.

As a first step, changes in oxygen levels as cells in culture respire must be examined. A number of oxygen sensors have been developed; however, they suffer from a wide variety of issues including invasiveness, lack of sensitivity, and incompatibility with microscopic imaging techniques. This causes oxygen measurements to be a stand-alone technique, which prevents their adoption and limits their applications and

significance in biology and cell culture. The focus of the current dissertation is to highlight the importance of oxygen measurement in cell culture through the development of a thin-film polymeric oxygen sensor that overcomes prior sensor deficiencies.

1.2 Proposed Approach

The studies completed in this dissertation center around the development and applications of an *in vitro* thin film oxygen sensor. The focus in each case is on the ability to non-invasively measure oxygen and integrate this technique into the different types of cell culture formats, thereby providing accurate information about oxygen levels in each system. In Chapter 2, we describe the background of phosphorescence quenching which is the basis of the current oxygen measurement technique. The different components that will be used during the fabrication steps of the oxygen sensor will be discussed. Finally, the characterization and data analysis techniques, which include phase-contrast and fluorescence microscopy and image normalization and analysis will be explained.

1.2.1 Development of Non-invasive Oxygen Sensors

Chapter 3 describes the development of a new non-invasive oxygen sensor that incorporates an oxygen sensitive dye, Pt(II) *meso*-Tetra(pentafluoro-phenyl)porphine (PtTFPP) into polydimethylsiloxane (PDMS) thin films. Using a multilayer design that sandwiches a thin Teflon AF film between the sensor layer (PtTFPP-PDMS) and cell culture layer (PDMS), dye cytotoxicity was effectively mitigated while providing a suitable substrate for cell attachment. A per-cell oxygen consumption rate for NIH 3T3

mouse fibroblasts was determined demonstrating the utility of this measurement. In addition, cells attached to the sensor were clearly visualized with both phase-contrast and fluorescence imaging, demonstrating facile integration into conventional microscopy techniques.

1.2.2 Oxygen Measurements in Hepatocyte Cultures

In the follow up study (Chapter 4), the oxygen environment in human hepatocarcinoma cell line HepG2 were characterized using the oxygen sensor. Oxygen measurements revealed the dynamic nature of oxygen levels in the culture and showed the cells were exposed to hypoxic conditions within 24 h after seeding. A per-cell oxygen consumption rate of 29 ± 6 fmol/min^{-1}·cell^{-1} was determined and reflected the high metabolic behavior of HepG2. Oxygen flux measurements indicated that at high densities, HepG2 cultures are oxygen starved and for a cell line that is widely used for toxicity screening, unwanted hypoxia-induced changes in cell behavior could potential alter testing results. Thus the current technique provides a useful tool to monitor how oxygen environment might change cell behavior in these high-respiring cell lines.

1.2.3 Oxygen Measurements in Microfluidic Systems

Finally, in Chapter 5, we expand the utility of this technology into microfluidic systems. The oxygen sensor was successfully integrated into a multilayer microfluidic device. With an off-chip gas exchanger, liquid with different dissolved oxygen content was introduced to regulate the oxygen levels on-chip. This method allows precise control of oxygen levels and eliminates pervaporation associated with previous devices. The

integrated oxygen sensor allows accurate real-time measurements of on-chip oxygen levels and the results were confirmed using numerical simulations. Besides quantifying the oxygen levels, this form of integrating measurement capabilities on-chip provides a new direction to non-invasively monitor the microenvironment within microfluidic systems.

1.3 Significance of This Work

The studies completed in this dissertation provide the proof of concept for a robust, non-invasive, microscopy-compatible oxygen sensor for use with cell culture. The simplicity of the current measurement and the ease of integration into different cell culture formats make our sensor a powerful tool for monitoring and quantifying the effects of oxygen levels in cell biology.

Chapter 2

Background

In this chapter, we will discuss the basics of phosphorescence and the theory behind phosphorescence quenching by oxygen. The method to characterize this quenching effect for oxygen measurements will also be described. In addition, the types of oxygen sensitive dyes and the polymers that were used to fabricate the sensors will be presented. Finally, we will finish with a short discussion on the different characterization techniques used, including phase and fluorescence microscopy and the basics of image analysis.

2.1 Phosphorescence

Prior to the discussion of phosphorescence, we will first briefly touch on the basics of fluorescence due to their overlapping theory. Both fluorescence and phosphorescence are categorized under luminescence which is the emission of photons from electronically excited states. In both of these processes, an outside energy source, light, must be absorbed which then results in the emission of another light. Light can be described as energy using Planck's law $E = h\nu$, therefore the Jablonski diagram[11] (Figure 2.1) is used to described the different energy levels that a molecule travels during and after energy absorption.

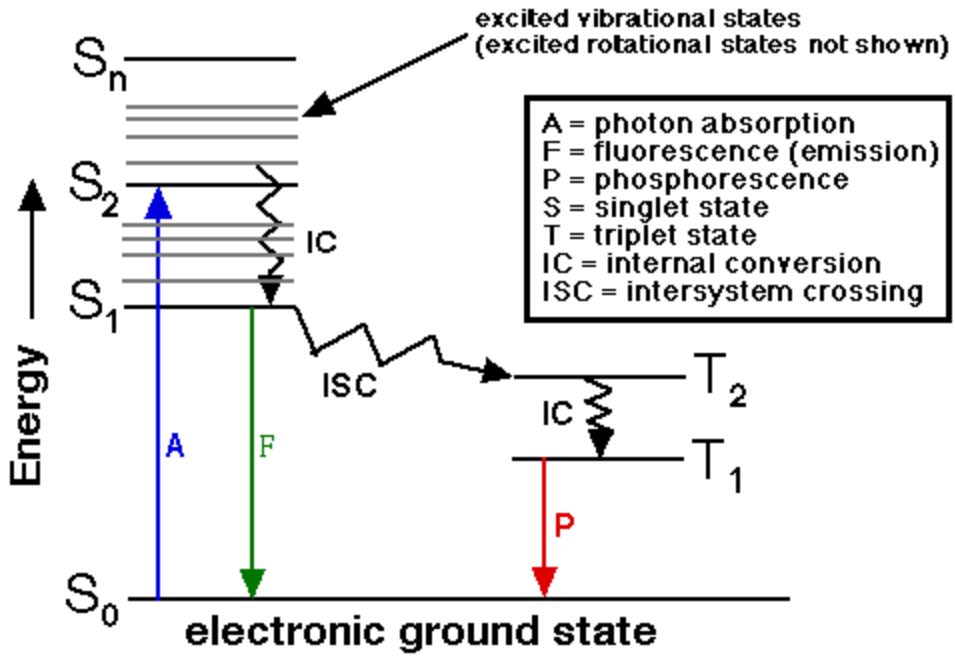

Figure 2.1.Simplified Jablonski diagram illustrating the different energy states involved light absorption and emission. Adapted from (www.shsu.edu/~chemistry)

As depicted by the Jablonski diagram (Figure 2.1), when a molecule absorbs energy, it jumps from the singlet ground state (S_0) to an excited singlet state (S_2). Internal conversion subsequently returns the molecule to the lowest excited state of S_1. The process by which the fluorophore returns from S_1 to S_0 with the emission of a photon (light at a different wavelength) is fluorescence.[12] In contrast, when molecules in S_1 undergo intersystem crossing to the triplet state T_1, the emission of photons back to the ground state S_0 is known as phosphorescence.[12] Under certain conditions, the phosphorescent molecule can return to the ground state without the emission of a photon. One process, known as quenching, occurs when the excited molecule collides with another molecule (quencher) resulting in the transfer of energy and relaxation without emission.[12]

In the current dissertation, we are focused on a class of dye molecules whose emission is quenched by the presence of molecular oxygen. Oxygen in its ground state is in a triplet and therefore, a molecule that crosses into excited triplet state can easily be quenched upon colliding with oxygen.[12,13]

2.2 Oxygen Sensitive Molecules

The dye molecule used in this study belongs to the class of phosphorescent metalloporphyrins, specifically platinum (Pt) porphyrins. In the excited triplet state, the dye emissions are effectively quenched by oxygen providing a suitable method for oxygen sensing. In general, Pt-porphyrins which has a platinum ion surrounded by porphyrin rings (Figure 2.2a) have an absorption wavelength at ~ 400 nm and an emission wavelength at ~ 650nm.[14] The presence of porphyrins and the heavy atom in the middle allow these molecules to efficiently cross into their triplet state. Pt-porphyrins are generally more stable compared to other metalloporphyrins because the Pt(II) ions do not easily dissociate from the molecule. This is because the Pt(II) ions require a planar geometry for stability, which is well provided by the porphyrin ring. Besides detecting oxygen, these dyes are also used as photosensitizers due to their efficient generation of singlet oxygen. The porphyrin used in this dissertation is Pt(II) *meso*-Tetra(pentafluorophenyl)porphine (Figure 2.2b) due to its favorable photostability.

(a)

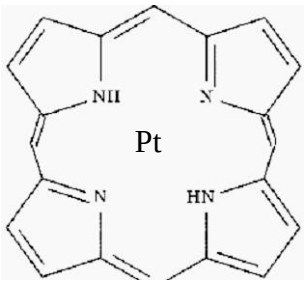

(b)

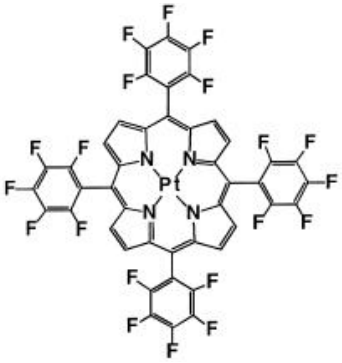

Figure 2.2 (a) Schematic of a metalloporphyrin with a porphyrin ring surrounding a Pt ion. Modifications can be made around the ring to enhance solubility in various solvents. (b) Chemical structure of Pt(II) *meso*-Tetra(pentafluorophenyl)porphine is shown.

2.3 Gas Permeable Polymers

Two type of polymers were used during the design of the oxygen sensors. Poly(dimethylsiloxane) (PDMS) and Teflon AF were chosen due to their high gas peremability and favorable optical characteristics (Figure 2.3).

- PDMS: This hydrophobic elastomer (Figure 2.3a) is one of the most gas permeable polymers that are commercially available. The permeabilites of PDMS to oxygen, nitrogen, and carbon dioxide are 800 Barrer, 400 Barrer, and 3800 Barrer, respectively, several orders of magnitude higher than glassy polymers such as polystyrene.[15] As such, they are widely used for commercial gas separation purposes.[16,17] The elastomer has low intermolecular forces and unhindered single bonds which results in high polymer chain mobility and higher than usual free volume, allowsing gas to freely diffuse through.[18] In addition, PDMS

is optically transparent and biocompatible making it a suitable substrate for cell based assays.[19]

- Teflon AF: This amorphous, glassy copolymer contains 87 mol% 2,2-bistrifluoromethyl-4,5-difluoro-1,3-dioxole and 13 mol% tetrafluoro-ethylene (Figure 2.3b). Similar to PDMS, it is highly gas permeable and the permeabilities to oxygen, nitrogen and carbon dioxide are: 1600 Barrer, 780 Barrer, and 3900 Barrer, respectively.[20] Teflon AF is dissolved in a perfluorated solvent and can be used for surface coatings.

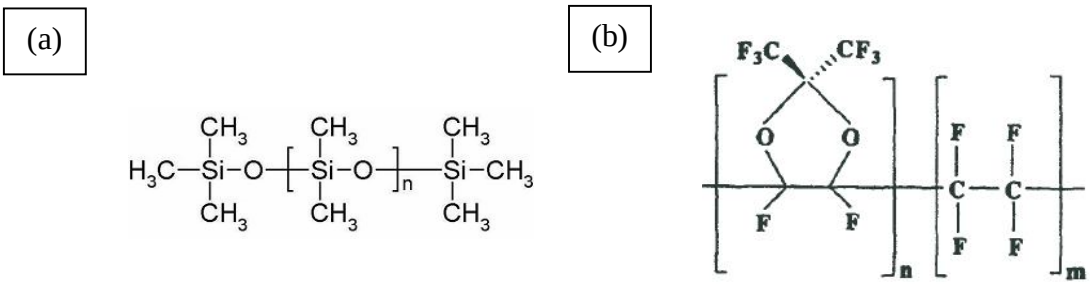

Figure 2.3 (a) Schematic of gas permeable polymers PDMS and (b) Teflon AF.

2.4 Stern-Volmer Relationship

In dynamic quenching, the excited molecule collides with a quencher and is returned to the ground state without the emission of a photon. The process of quenching therefore is in competition with other modes of relaxation, including luminescence (photon emission) and vibrational relaxation (return to the ground state by emission of heat). This suggests that, depending on the amount of quencher present, photon emission by the dye will vary based on these competing mechanisms. Using oxygen as a quencher, these three mechanisms can be written as the following rate equations:

Excitation of a phosphorescent dye by a photon ($h\nu_1$) with a rate constant k_1:

$$\text{Dye} + h\upsilon_1 \xrightarrow{k_1} \text{Dye}^* \tag{2.4.1}$$

In the excited state, dye can relax back to the ground state by photon emission with a rate constant k_{ph}:

$$\text{Dye}^* \xrightarrow{k_{ph}} \text{Dye} + h\upsilon_2 \tag{2.4.2}$$

Relaxation to the ground state can also occur through release of heat instead of photons. The rate constant for the process is k_h:

$$\text{Dye}^* \xrightarrow{k_h} \text{Dye} + \text{heat} \tag{2.4.3}$$

In the presence of oxygen (quencher), the molecule returns to the ground state without photon emission. Rate constant for this process is k_q

$$\text{Dye}^* + \text{O}_2 \xrightarrow{k_q} \text{Dye} + \text{O}_2^* \tag{2.4.4}$$

The intensity that will be measured from the phosphorescent dye will depend on the amount of photons ($h\nu_2$) emitted. Therefore the equation for the intensity is:

$$I = \frac{d[h\upsilon_2]}{dt} = k_{ph} \cdot [\text{Dye}^*] \tag{2.4.5}$$

The change in the concentration of excited state dye ([Dye*]) with time is written as the sum of all the processes (eq 2.4.1-4) that contribute to the formation and elimination of Dye*:

$$\frac{d[\text{Dye}^*]}{dt} = k_1[\text{Dye}][h\upsilon_1] - k_{ph}[\text{Dye}^*] - k_h[\text{Dye}^*] - k_q[\text{Dye}^*][\text{O}_2] \tag{2.4.6}$$

Using the pseudo-steady-state assumption, i.e., that Dye* is a short-lived intermediate, we can put $\frac{d[\text{Dye}^*]}{dt} = 0$. Eq (2.4.6) can then be ararranged into:

$$[\text{Dye}^*] = \frac{k_1[\text{Dye}][h\upsilon_1]}{k_{ph} + k_h + k_q[\text{O}_2]} \tag{2.4.7}$$

By combining equations (2.4.5) and (2.4.7):

$$I = k_{ph} * \frac{k_1[\text{Dye}][h\upsilon_1]}{k_{ph} + k_h + k_q[\text{O}_2]} \tag{2.4.8}$$

In the absence of oxygen, the intensity emitted can be written as:

$$I(\text{O}_2 = 0) = I_0 = k_{ph} * \frac{k_1[\text{Dye}][h\upsilon_1]}{k_{ph} + k_h} \tag{2.4.9}$$

Diving equation (2.4.9) by equation (2.4.8), the result is

$$\frac{I_0}{I} = 1 + \frac{k_q}{k_{ph} + k_h}[\text{O}_2] = 1 + k_{\text{SV}} \cdot [\text{O}_2] \tag{2.4.10}$$

Equation (2.4.10) is known as the Stern-Volmer equation[21-24] and it is used to describe the variation in the phorphorescence emission (or fluorescence) in the presence of oxygen. This equation implies a linear relationship between the oxygen concentration and the reciprocal of the intensity. The slope of the line is the Stern-Volmer constant K_{SV}. A linear Stern-Volmer plot generally implies that the fluorophores are equally accessible to the quencher. Deviations from linearity occur when there are more than one class of fluorophores where one is accessible to the quencher while the other is not.[12] This frequently occurs in polymeric sensors where phosphorescent dyes are not homogeneously distributed throughout the film and dye aggregation occurs. As such, this relationship must first be validated before a given dye is used for oxygen measurement.

2.5 Optical Microscopy: Phase Contrast, Fluorescence

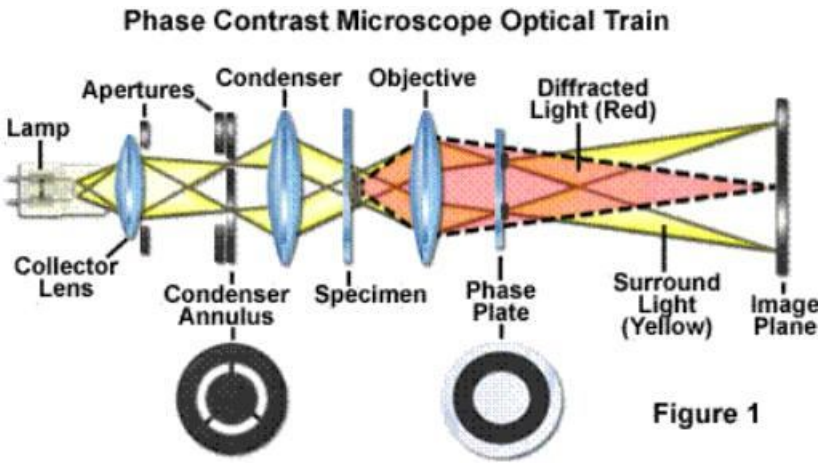

Figure 2.4 Schematic demonstrating the path of light in phase contrast microscopy (from www.microscopy.com).

Phase-contrast microscopy, a technique frequently used to image cells, utilizes the relationship between diffracted light from the sample and undiffracted background light.[25] In general, when light passes through an object, it is slowed down by ¼ of a wavelength in comparison with the undiffracted background light. However, ½ of a wavelength phase shift is needed in order to produce destructive interference that result in contrasting imaging. Based on this concept, the main components of a phase contrast microscope consist of an annular ring in the condenser and a phase plate in the back focal plane of the objective to achieve the required phase shift (Figure 2.4). The annular ring controls where the undiffracted background light will go. Undiffracted light, after passing through the plane of the sample, will focus on the back focal plane of the objective where it encounters the phase plate. The phase plate is modified to allow this light to travel through with a ¼ wavelength jump relative to the diffracted light from the sample. The resulting two ¼ wavelength differences (¼ wavelength for sample diffraction and ¼ from

phase plate) is combined to produce ½ of a wavelength phase shift to produce the contrasting image.

Fluorescence microscopy is another technique used in cell measurements. In this work, we will use reflected-light fluorescence microscopy to measure the varying intensity of phosphorescence as our dye is quenched. The basic components of fluorescence imaging consist of a light source, a dichromatic light splitter, objective, and the detector. Excitation light, with short wavelength and high energy, is reflected by the dichromatic beam splitter through the objective and onto the sample. Upon excitation, the sample emits fluorescence in a lower energy wavelength which is then collected by the objective, passes through the dichromatic mirror and is quantified by the detector.

2.6 Image Analysis

The most common fluorescent light source is the mercury (Hg) arc lamp. The high intensity light generated by this lamp is derived from the Hg light bulb which consists of two electrodes that are sealed under pressure and surrounded by Hg. The lamp is ignited when high voltage ionizes the Hg within the bulb thus turning it on. During operation, these ions carry a current between the two electrodes generating an arc of current, or light that is used to excite a fluorescent specimen. In general, an image obtained this way will have a brighter intensity in the middle of the field of view compared to the edges due to the focusing optics involved. To account for the spatial variation in incident intensity (which directly impacts the resulting fluorescence intensity), all quantitative images have to be “flat field corrected”, i.e., intensity artifacts

must be removed to give a uniform (flat) image intensity, by dividing each raw image by a control image. For a raw fluorescent image having an intensity image matrix of $I_{raw}[x,y]$, flat field correction is performed using the following equation:

$$I_{flat}[x,y] = \frac{I_{raw}[x,y] - I_{darkcount}[x,y]}{I_{control}[x,y] - I_{darkcount}[x,y]} \quad (2.6.1)$$

In addition, the baseline intensity contributed by the background must be eliminated to ensure that any change in intensity is only a result of the specimen itself. In this case, background intensity is generated from the dark counts ($I_{darkcount}[x,y]$) of the CCD camera systems and all other intensity ($I_{background}[x,y]$) in the field of view excluding the dye. Therefore to ensure that only on the intensity emitted from the dye is measured, background subtraction needs to be performed on the flattened image ($I_{flat}[x,y]$) using the following equation:

$$I_{dye}[x,y] = I_{flat}[x,y] - I_{darkcount}[x,y] - I_{background}[x,y] \quad (2.6.2)$$

Chapter 3

Development of Non-Invasive Oxygen Sensors

The results presented in this chapter have been published in the following journal article: Peter C. Thomas, Michael Halter, Alessandro Tona, Srinivasa R. Raghavan, Anne L. Plant and Samuel P. Forry, *"A Noninvasive Thin Film Sensor for Monitoring Oxygen Tension during In Vitro Cell Culture"* Analytical Chemistry **2009**, 81, 9239-9246

3.1 Introduction

In vivo, oxygen levels vary across a wide spectrum. While atmospheric oxygen enters the lungs at an oxygen partial pressure of 21% (P_{O2} = 0.21 atm = 2.1 × 10^4 Pa), the oxygen level decreases as it circulates through the body, reaching a mean oxygen level in tissue of ~ 3-5% (P_{O2} = 0.03-0.05 atm).[10,26] In addition, some cells experience a dynamic oxygen environment. For example, hepatocytes *in vivo* are exposed to gradients of oxygen[27,28] while immune cells encounter different oxygen levels as they migrate through different tissues.[29] The variations of oxygen level throughout the body can significantly impact disease and wound healing processes. For instance, low oxygen levels mark the onset of wound healing process, but prolonged hypoxia will eventually lead to non-healing wounds.[30] An *in vitro* study demonstrated how low oxygen levels lead to vasoocclusion in sickle cell anemia.[31] Cancer cells that exist in hypoxic conditions are characterized as more virulent and more resistant to radiotherapy.[32]

Despite the significance of oxygen tension *in vivo*, conventional cell culture methods rarely specify oxygen levels and most *in vitro* cell cultures are still performed at atmospheric oxygen levels (P_{O2} = 0.21 atm). There are many reported examples where the disparity between *in vivo* and *in vitro* oxygen levels resulted in misleading experimental conclusions. For example, *in vitro* studies of stem cells have demonstrated greater proliferation[10] and reduced spontaneous differentiation[33] at physiological oxygen tension (P_{O2}= 0.05 atm), as well as oxygen tension-dependent differentiation pathways.[34] Similarly the oxygen tension during cell culture has been shown to alter the intracellular redox state of T cells[26] and to affect the response of lymphocytes toward HIV viral protein.[35] Hepatocyte cultures must be exposed to a gradient of oxygen instead of a uniform oxygen tension in order to mimic the *in vivo* compartmentalization of liver.[27,28] These findings point to the critical need to monitor and control oxygen tension in cell cultures.

During *in vitro* culture, oxygen is locally consumed by the cells and is replenished through equilibrium with the bulk culture medium. However, at high cell densities or long culture periods, depletion can lead to changes in bulk oxygen tension. Therefore, real time measurement strategies are needed to continuously monitor oxygen levels. Indeed, changes in the rate of oxygen consumption in cell culture can also provide a direct measurement of cellular metabolic activity. Traditionally, the Clark electrode has been utilized to monitor oxygen.[36,37] However, since the electrode consumes oxygen during measurement it can potentially alter the oxygen concentration in culture. Also, for real-time measurements, the electrode has to be placed inside the culture chamber,

creating a source of contamination for the culture and complicating simultaneous imaging of the cells. Spectroscopic techniques can provide less invasive methods of measuring the oxygen tension, based on the quenching of phosphorescent molecules. For example, Ruthenium (II) complexes loaded in polymeric beads[38] or on microplates[39,40] can be used for continuous oxygen measurements. Also, oxygen probes synthesized by conjugating an oxygen-sensitive dye to macromolecular carriers (e.g. PEG or BSA) have been used to measure oxygen levels in cell culture.[41] Previously, these approaches have been relatively incompatible with imaging and these sensors have been stand-alone, rather than integrated, measurements. In addition, low oxygen sensitivity, significant photobleaching during long culture periods and possible fouling of the probes by the surrounding culture medium have limited widespread implementation.

In this report we describe a thin film polymeric sensor for making sensitive real-time oxygen measurement that is compatible with phase contrast and fluorescence microscopy of cells. The principle of the sensor is based on the oxygen-dependent quenching of phosphorescence from a platinum porphyrin dye embedded within a gas permeable film. We have developed a multi-layer design that prevents leakage of dye into the cells and thereby eliminates issues related to dye cytotoxicity, while still maintaining high sensor sensitivity. To demonstrate the utility of the sensor, we have continuously monitored changes in oxygen tension during long-term cell culture experiments for NIH 3T3 mouse fibroblasts. The data were used to determine the per-cell rate of oxygen consumption for the case of the NIH 3T3 fibroblasts.

3.2 Experimental Methods

Cell Culture Human umbilical vein endothelial cells (HUVEC) (ATCC, Manassas, VA) were cultured in F12K Medium (ATCC), supplemented with 0.1 mg/mL heparins (Sigma, St. Louis, MO), 0.03 mg/mL Endothelial Cell Growth Supplement (Sigma) and 10% (v/v) fetal bovine serum. NIH 3T3 mouse fibroblasts (ATCC, Manassas, VA) were cultured in Dulbecco's Modified Eagles Medium (DMEM; Mediatech, Herndon, VA) supplemented with 10% (v/v) fetal bovine serum and the non essential amino acids and glutamine (4 mmol/L). Both cell lines were maintained in humidified air balanced with 5% (v/v) CO_2 at 37°C. Unless otherwise stated, cells were maintained inside the incubator until experiments began.

Cell Staining Live/Dead Viability/Cytotoxicity Kit (L-3224) assay and Hoechst 33342 stain (both from Invitrogen Corporation, Carlsbad, CA) were done according to the manufacturer's direction. For the Live/Dead assay, calcein AM (4 mmol/L) and ethidium homodimer-1 (2 mmol/L) were diluted in culture medium to get a final concentration of 1 μmol/L and 4 μmol/L, respectively. Cells were washed with phosphate-buffered saline (PBS) twice, and the stain solution was added. Cells and stain were then placed in the incubator for 30 min before being imaged. For nuclear staining with Hoechst 33242, the dye was dissolved in DMEM and an equivalent volume of dye solution was added to each cell culture well resulting in a concentration of 2 μg/mL Hoechst 33342. Cells were imaged without rinsing after 15 min of incubation with the staining solution.

Sensor Preparation Two oxygen sensor compositions were explored in this study. The first sensor consisted of the porphyrin dye Pt(II) meso-Tetra(pentafluorophenyl)porphine (PtTFPP, Frontier Scientific Inc, Logan, Utah) dissolved in toluene and thoroughly mixed with a 10:1 ratio of polydimethylsiloxane prepolymer:curing agent solution (PDMS, Slygard 184; Dow-Corning, Midland, MI) and spin coated onto 18 mm glass coverslips. Toluene was allowed to evaporate overnight while the polymer cured. The final PtTFPP sensor film had a dye concentration of 1 mmol/L and was 66 μm thick. The second composition consisted of a three layer sensor (PtTFPP-Tef-PDMS) prepared by spin coating Teflon AF (Dow Chemical) onto the PtTFPP sensor films described previously and allowing solvents to evaporate overnight. Finally, an additional film of PDMS without dye was spin coated and cured on top of the Teflon. All sensor formulation covered the entire surface of the coverslip with an area of 2.54 cm^2. The final thickness of the PtTFPP-Tef-PDMS film was approximately 150 μm. Sensor thickness was measured using an optical profiler (WYKO NT100 DMEM; Veeco, Tucson, AZ). Sensors were stored in the dark and used within 2 weeks of being made; new sensors were used for each experiment. The fabrication strategy (spin coating sequential sensor layers) could be rapidly adapted to a variety of sensor geometries. This sensor formulation was not optimized but was used consistently throughout this work. Ongoing efforts focus on sensor design optimization

Sensor Calibration PtTFPP sensor and PtTFPP-Tef-PDMS films were placed inside a multi-well dish modified to allow continuous gas flow (0%, 5%, 10%, 15%, or 21% O_2 in N_2; Scotts Specialty Gas; Plumsteadville, PA) through the dish headspace. Oxygen flux

through the dish material (polystyrene) was minimal ($D_{O2\ in\ PS} \approx 10^{-7}$ cm^2s^{-1}) and was ignored. While controlling the headspace composition, the PtTFPP emission intensity was captured using a 10× (0.3NA) objective on an inverted microscope (Zeiss Axiovert 200, Thornwood, NJ) with the focus placed on the surface of the sensor (Figure 3.1a). The films were illuminated with an X-Cite metal halide light source (EXFO, Ontario, Canada) at 546±6 nm and the emission was captured using a 580 nm dichroic, a Color IEEE-1394 camera (Scion Corporation, Frederick, MD) with an integration time of 70 ms, and a long pass emission filter with a 590 nm cutoff.

All images were analyzed using NIH ImageJ (http://rsbweb.nih.gov/ij/) software. Blank PDMS films (without PtTFPP) spun to the same thickness as the oxygen sensors were also imaged to account for background intensity. These intensity values were subtracted from all sensor images in order to obtain the actual intensity from the dye itself. To determine the sensor response, Ksv was calculated from a linear regression using the Stern-Volmer equation. The reported mean Ksv and standard deviation were determined from 29 positions on 14 different sensors. To measure the dissolved oxygen in solution, culture medium without phenol red was added on top of the oxygen sensor, and gas was introduced as described above to control the headspace composition.

Sensor Preparation for Cell Culture The oxygen sensor was bonded to the inside of a 12 well cell culture plate with 0.5 μL of PDMS. Prior to cell seeding, the sensor was cleaned with 70% ethanol and rinsed with PBS. Bovine fibronectin solution (Sigma, St. Louis, MO) was diluted with PBS to 25 μg/mL and added to the culture well for 1 h to

facilitate cell attachment. The fibronectin solution was aspirated and freshly trypsinized cells (HUVEC or NIH 3T3) were subsequently seeded on the fibronectin-coated sensor.

Cytoxoticity Study NIH 3T3 cells were seeded at 60 cells/mm^2 on fibronectin treated films and allowed to attach overnight in 1 mL phenol red free culture medium to minimize background fluorescence. Cells were exposed to fluorescent excitation light with an integration time of 70 ms every 15 min for 3.5 h. Live/Dead cell assays were performed as described above on PDMS, PtTFPP sensors, and PtTFPP-Tef-PDMS and 5 positions were selected and imaged, with all conditions evaluated in triplicate. Live cells were imaged and counted with an excitation wavelength of 470 nm and emission of 540 nm. Dead cells were imaged and counted using a filter cube with excitation at 546 nm and emission at 590 nm. Total viable cells were reported by dividing the number of live cells over the total cell count for each position.

Oxygen Measurement in Cell Culture NIH 3T3 or HUVEC cells were seeded on sensors prepared for cell culture and allowed to attach over night in 1 mL of culture medium without phenol red. Cells were placed on an inverted Axiovert 200M microscope (Zeiss, Thornwood, NJ) with an automated stage (Ludl, Hawthorone, NY) and maintained at 37^{o}C in a microscope incubator (In Vivo Scientific) attached to the microscope.

In initial experiments, the P_{O_2} in the headspace above the cell culture medium was controlled as described in the sensor calibration section. For subsequent experiments

during extended cell culture, cells were maintained on the microscope throughout the experiment. The culture headspace was maintained with humidified 5% CO_2 in balanced air (In Vivo Scientific) and maintained at 37°C as described above. Cells were cultured in 3 mL of culture medium without phenol red. Image capture began immediately after seeding. Prior to the start of each experiment, 3 positions were selected in each well. All experiments were performed in triplicate; control wells contained medium without cells. Under these conditions, the doubling time of NIH 3T3 cells was ≈ 20 h.

3.3 Results and Discussion

Sensor Calibration in Gas and Liquid. The phosphorescent platinum porphyrin dye Pt(II) meso-Tetra(pentafluorophenyl) porphine (PtTFPP) has been used previously to measure the partial pressure of oxygen due to its compatibility with common polymers and a lack of photobleaching.[14,42,43] In the current study, PtTFPP was dissolved in a gas permeable PDMS polymer matrix that was spin coated to form thin film oxygen sensors (this sensor formulation is referred to as PtTFPP sensor). This thin film geometry allowed rapid diffusion of oxygen throughout the dye-filled matrix. As expected, the phosphorescence from PtTFPP sensor was significantly quenched in the presence of oxygen gas (Figure 3.1b). The quenching response followed the Stern-Volmer equation:[12]

$$\frac{I_0}{I} = 1 + K_{SV} \cdot [P_{O_2}] \qquad (3.3.1)$$

where I is the phosphorescence intensity, I_0 is the intensity in the absence of oxygen, K_{SV} is the Stern-Volmer constant and P_{O2} is the partial pressure of oxygen in the gas phase. Thus, a plot of I_0/I vs. P_{O2} follows a straight line (Figure 3.1b). From the slope, K_{SV} = 584

± 71 atm^{-1} (mean and standard deviation of 14 different films). As expected, the sensor response was less reproducible at higher oxygen levels where significant quenching results in low emission intensity. This as evident in the relative large standard deviation at atmospheric oxygen conditions. However, the K_{SV} value for this oxygen sensor was much higher than values reported for other dyes, yielding a sensor with greater sensitivity than previously reported formulations.[39,44-46]

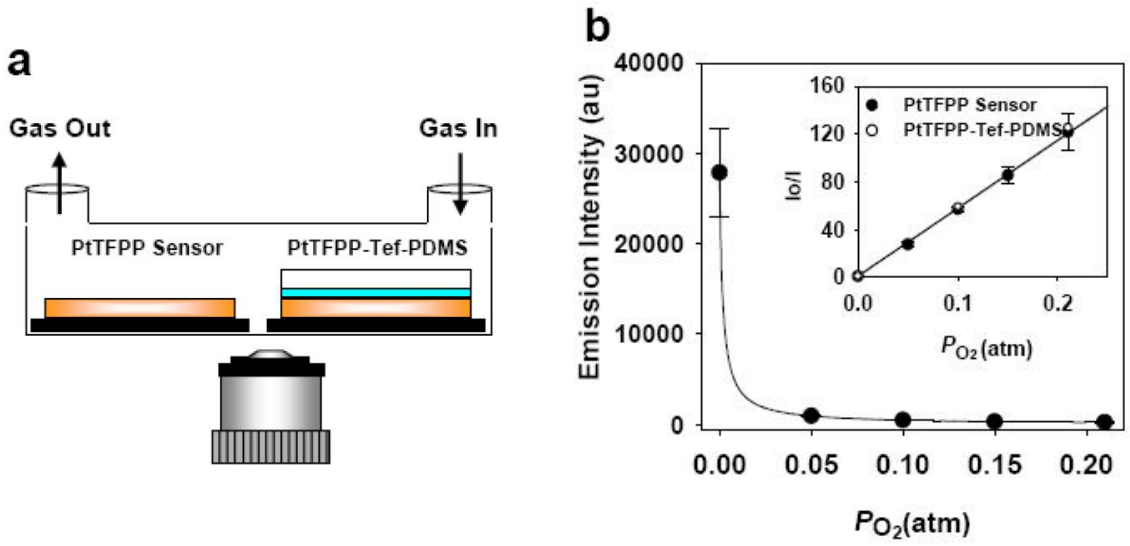

.

Figure 3.1 Gas phase calibration of the thin film PtTFPP and PtTFPP-Tef-PDMS oxygen sensors. The experimental setup for acquiring P_{O2} measurements on an inverted microscope at controlled gas compositions is shown schematically (a). The phosphorescent oxygen sensors exhibited significant quenching in the presence of oxygen (b), and followed the Stern-Volmer equation (inset) with high linearity and sensitivity (Ksv = 584 ± 71 atm^{-1}). Black circles represent PtTFPP sensors (n=4) and open circles represent PtTFPP-Tef-PDMS (n=10) films. Data points indicate the mean values from the sensor films with standard deviations given by the vertical error bars; solid lines indicate the best fit to the data using the Stern-Volmer relationship.

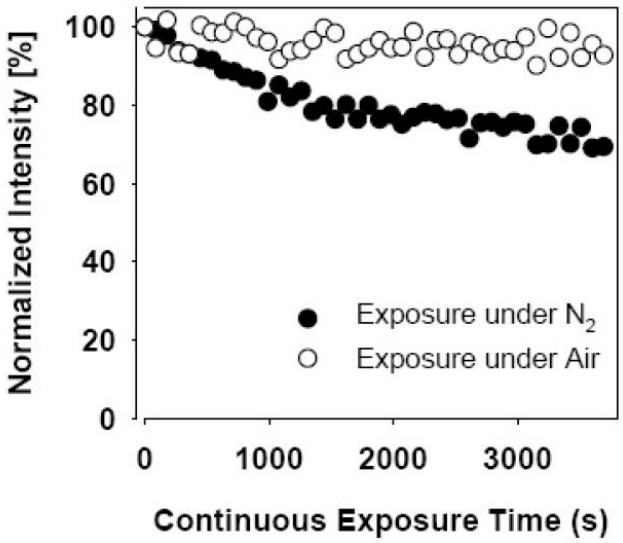

Figure 3.2 Photodegradation of oxygen sensor under continuous light exposure. PtTFPP sensor under continuous exposure of phosphorescent excitation for 3600 seconds in Air (open circles) showed negligible photobleaching effects and in pure N_2 (closed circles) showed a reduction of intensity by 30%. Images were taken every 90s. All images were normalized against the first image of the data set. During P_{O2} measurements, only a 70ms exposure was required. Even for the longest oxygen measurement experiments, the total integrated sensing time was less than 10 s.

In a second sensor formulation, thin layers of Teflon AF and PDMS without dye were spin coated on top of the PtTFPP sensor (the resulting sensor is denoted as PtTFPP-Tef-PDMS). The presence of the thin Teflon layer did not alter the response of PtTFPP-Tef-PDMS sensor towards oxygen compared to the PtTFPP sensors (Figure 3.1b, open circles), but did sequester the dye away from the sensor surface. For both sensor formulations, equilibrium was faster than the time required to change the headspace gas composition (<1 min), reflecting the high permeability of both Teflon AF (1500 Barrer) and PDMS (800 Barrer).[15,47]

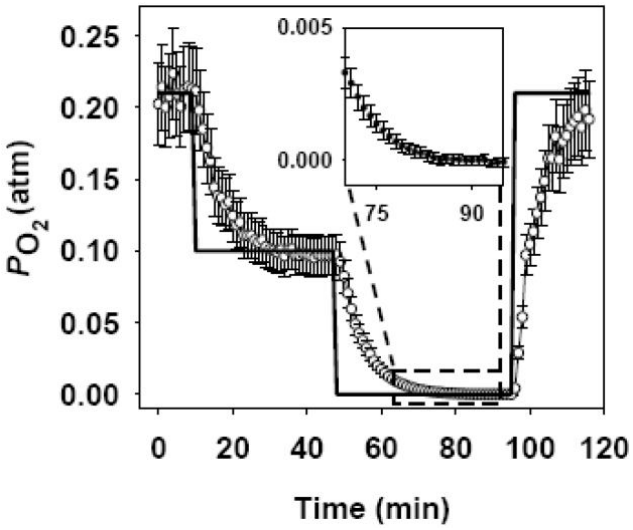

Figure 3.3 Performance of the oxygen sensor in cell culture medium. The oxygen tension in solution was measured (open circles) following step changes in the headspace gas composition (solid trace). The inset shows that the oxygen level in solution eventually decreased to 0 atm (within error) when pure N_2 was present in the headspace. Vertical error bars indicated the standard deviation in *K*sv and I_0 used to calculate P_{O2}.

Previous oxygen sensors based on the quenching of ruthenium complexes exhibited lower K_{SV} values (0.2 – 40 atm^{-1}) and were confounded by issues of dye aggregation.[39,44-46] Those dyes were relatively polar and ionic leading to low solubility and aggregation in nonpolar polymer matrices (e.g. PDMS). Dye aggregation has been associated with high variability in oxygen response, non-linear Stern-Volmer plots and uneven background emission that limits integration.[45,46] In comparison with previous dyes, the PtTFPP dye was relatively nonpolar and readily dissolved in the PDMS polymer matrix without dye aggregation or phase separation. As a result, the PtTFPP-based sensors exhibited a homogenous intensity and its response to P_{O2} levels followed the Stern-Volmer relationship. Additionally, no significant photobleaching effects were observed even during continuous illumination for > 3600 s (Figure 3.2).

Next, the PtTFPP sensor was placed at the bottom of a multi-well dish filled with cell culture medium. The oxygen partial pressure within the multi-well dish headspace was decreased in steps. After each step, the amount of dissolved oxygen in solution gradually decreased as it equilibrated with the controlled headspace composition. The rapid PtTFPP sensor equilibration (<1 min) allowed this transient behavior in solution to be monitored in real time (Figure 3.3).

The sensor calibration yielded a measurement of gas phase oxygen partial pressure even though it is the dissolved oxygen within the PDMS that actually quenches the PtTFPP dye. This calibration assumes that the sensor equilibrates rapidly with the adjacent medium so that the oxygen concentration in the PDMS is always proportional to the P_{O2} in the gas phase. For solution phase measurements, the rapid sensor equilibrium ensures accurate measurement of the dissolved oxygen in solution, and the calculated oxygen level reports the gas phase P_{O2} (in atm) that would yield an identical oxygen concentration (in mol/L) at equilibrium. This was verified in Figure 3.3 when the solution was allowed to equilibrate, and the resulting oxygen measurement matched the controlled headspace composition. These units are interchangeable using the Henry's Law Constant for oxygen in water ($H_{O2\ in\ H2O}$ = 933 L·atm/mol at 37°C).[48] The gas phase P_{O2} was reported here even for aqueous phase measurements as is conventional for reporting oxygen tension.

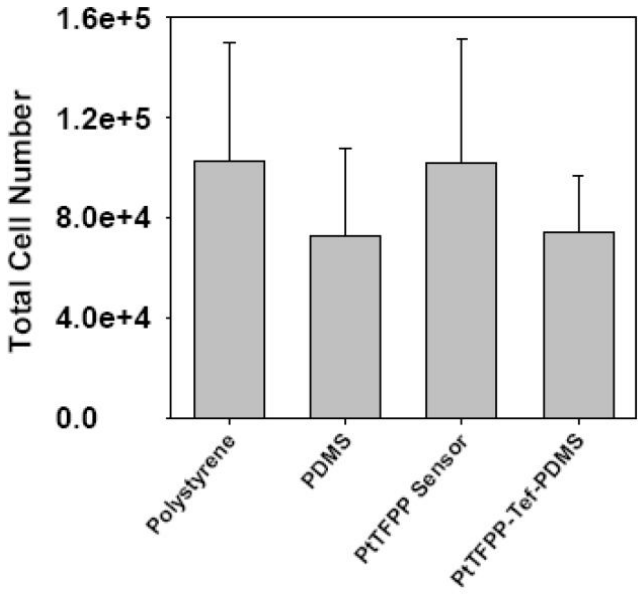

Figure 3.4 Proliferation of cells on various substrates. NIH 3T3 mouse fibroblasts were seeded (60 cells/mm^2) on 4 different fibronectin coated surfaces (polystyrene, PDMS films, PtTFPP sensor and PtTFPP-Tef-PDMS sensor) and allowed to proliferate for 70 hrs in the incubator (in darkness). Cells were subsequently trypsinized and counted. No statistically significant difference was observed between the different surfaces. Error bars depict the mean and standard deviation from triplicate experiments. No statistically significant difference was observed between the different surfaces ($p = 0.72$).

Sensor Cytotoxicity Studies. Cell viability assays were performed with NIH 3T3 cells to identify any potential cytotoxic effects with the sensors. All sensor films were coated with fibronectin to facilitate cell attachment. In the absence of illumination, cells proliferated as well on the PtTFPP-based sensors as on polystyrene culture dishes (Figure 3.4). However, upon exposure to phosphorescent excitation (546 nm for 0.07 s every 15 min for 3.5 h), cells on PtTFPP sensors were observed by phase microscopy to round up and detach (Figure 3.5a). A Live/Dead assay utilizing calcein AM to stain live cells and ethidium homodimer to stain dead cells confirmed significant phototoxicity for the PtTFPP sensor (Figure 3.5b-c). Cells attached to PDMS without PtTFPP proliferated normally and no phototoxicity was observed (Figure 3.5b-c). , The excited PtTFPP has

been shown previously to produce reactive oxygen species (ROS) when quenched by oxygen.[49] The short lifetime of these reactive species should preclude them diffusing out of the sensor after illumination. However, the PtTFPP dye itself may escape from the PtTFPP sensors and partition into the cell membranes, leading to ROS generation locally and the observed phototoxicity. In the second sensor formulation, PtTFPP-Tef-PDMS, phototoxicity was mitigated. Here a thin Teflon AF layer was added on top of the PtTFPP sensor, followed by a second PDMS layer without dye. We hypothesize that while oxygen diffuses easily through the Teflon layer, the PtTFPP would be effectively blocked due to the low diffusivity of larger molecules through Teflon AF.[50] The second PDMS layer was added to facilitate protein adsorption and cell attachment. Cells cultured on the PtTFPP-Tef-PDMS sensor (Figure 3.5a) exhibited similar morphology to cells on just PDMS. Quantification of the Live/Dead assay (Figure 3.5d) confirmed that the phototoxicity was completely mitigated with the PtTFPP-Tef-PDMS formulation.

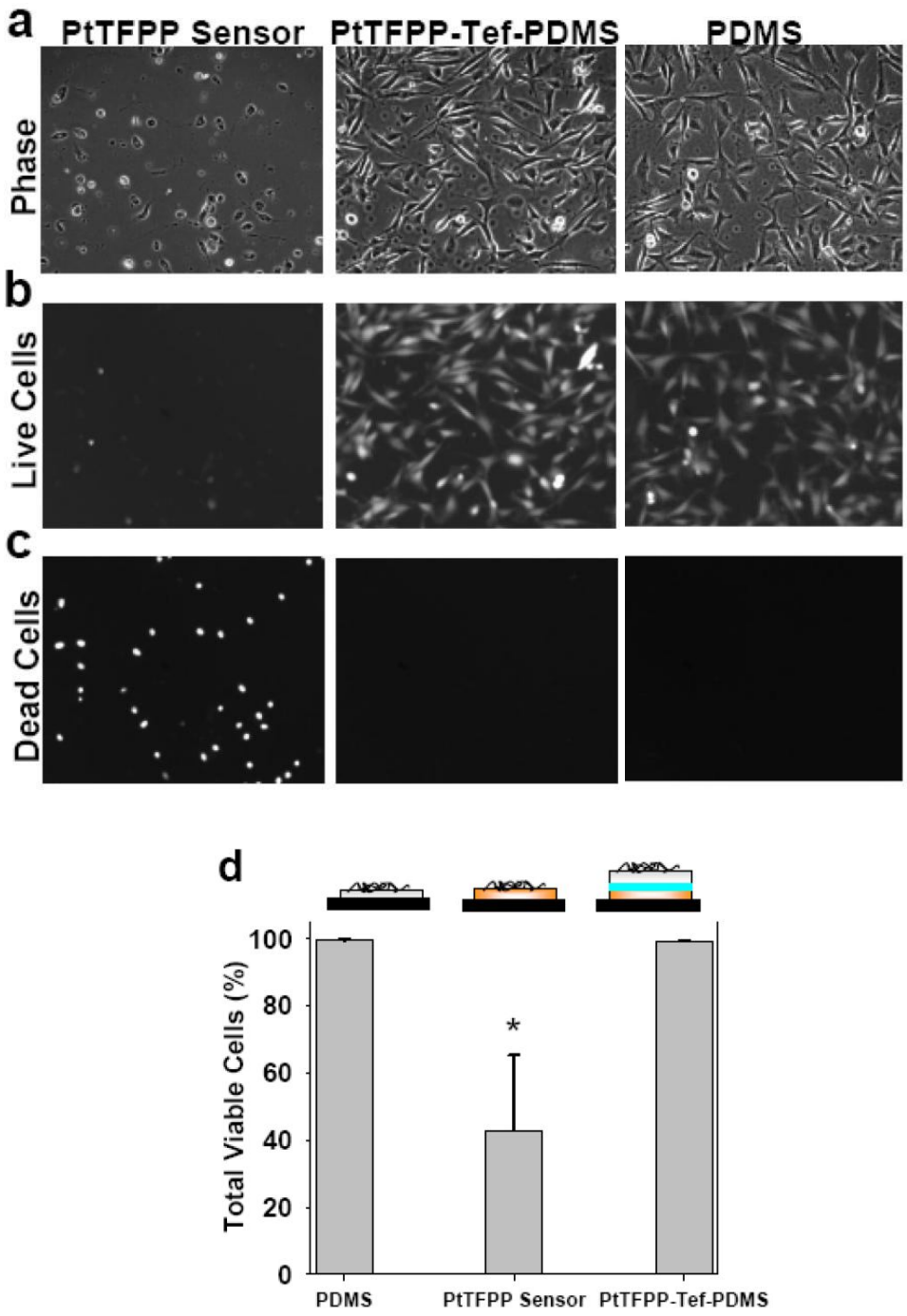

Figure 3.5 Phototoxicity of sensor formulations. NIH 3T3 cells were cultured on three surfaces (PDMS, PtTFPP sensor, and PtTFPP-Tef-PDMS) exposed to 70 ms exposures of 546 nm light every 15 min for 3.5 h and evaluated by phase contrast imaging (a) as well as by Live/Dead assays (b,c). Significant phototoxicity was observed on the PtTFPP sensor as compared to PDMS without dye, but the three-layer sensor mitigated the phototoxic effects. The percentage of viable cells was quantified for each substrate (d) and a 2-tail t-test was used to compare each sensor formulation to the PDMS without dye (* indicates $p < 0.05$). Columns and error bars indicate mean and standard deviation from triplicate experiments.

All of the sensor films (including the non-toxic PtTFPP-Tef-PDMS formulation) were compatible with common microscope methods, allowing oxygen sensing and microscopy to be performed simultaneously. Using phase microscopy, cell motility as well as filopodia movement were easily observed through time-lapsed imaging. Likewise, the fluorescence from cells stained with calcein AM and ethidium homodimer in the Live/Dead assay was easily visualized. Even though the emission wavelengths of the PtTFPP and the ethidium homodimer overlapped, the PtTFPP dye was homogenous throughout the sensor film while the cell stain was localized in the fixed cells, enabling facile discrimination (Figure 3.6). It should be noted that such microscopic evaluations on cells would have been difficult or impossible to perform with previous oxygen sensor designs but were easily accomplished using the current thin film sensors.

Figure 3.6 Integration of oxygen sensor and fluorescent cell stains. Representative fluorescent image of blank PDMS films showed minimal background emission (a). The PtTFPP sensor without cells showed an emission that was homogeneous in intensity throughout the field of view (b). On the same senosro formuation, dead cells (NIH 3T3 fibroblasts) stained with ethidium homodimer generated local bright spots that were clearly visible over the PtTFPP emission (c) even though the emission wavelengths of the film and stain overlapped.

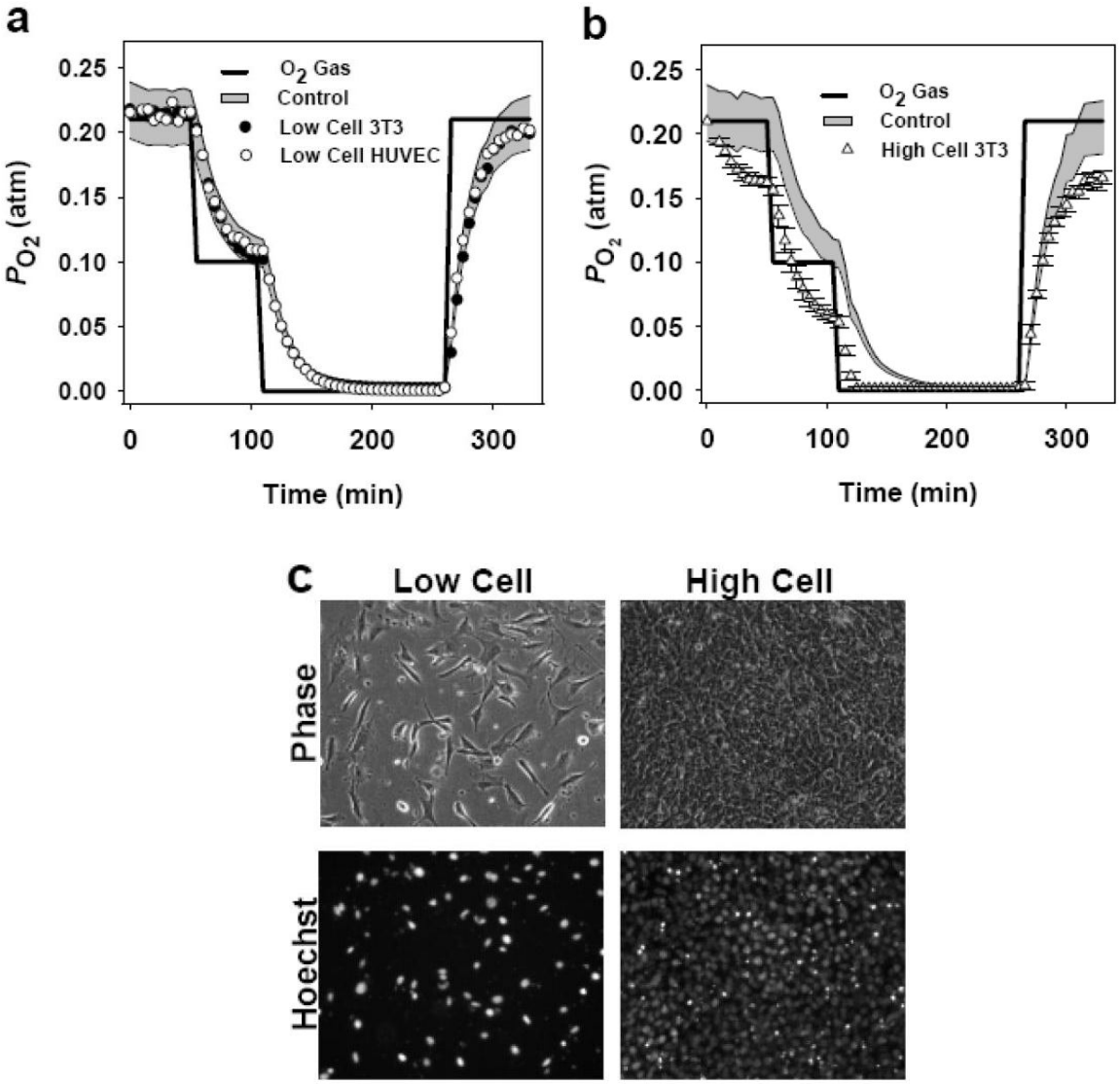

Figure 3.7 Oxygen measurements in the presence of live mammalian cells. At low cell seeding density (60 cells/mm^2) of HUVEC (open circles) or NIH 3T3 (black circles), the P_{O2} measured in culture was not statistically different from the control well (shaded region) that contained no cells (a). At high cell densities (3100 cells/mm^2, open triangles), the measured P_{O2} was significantly lower than the control throughout the experiment, indicating oxygen consumption by the cells (b). Representative phase contrast and Hoechst nuclear stained fluorescent microscopy images of NIH 3T3 cells on the PtTFPP-Tef-PDMS oxygen sensor are shown at low and high densities (c). The shaded region in (a) and (b) shows the 95% confidence interval envelope based on the uncertainty in measuring K_{sv} and I_0. Data points and error bars in (b) represent means and standard deviations from triplicate experiments.

Monitoring O_2 During Live Cell Culture. NIH 3T3 and HUVEC cells were seeded at very low densities on separate PtTFPP-Tef-PDMS sensors and allowed to attach and spread overnight. Subsequently, the P_{O2} in the cell culture was monitored following step changes in the head space gas composition to verify that oxygen measurements could be made during active cell culture. All culture medium was replaced prior to the start of the experiment to ensure that the P_{O2} levels in all chambers were 0.21 atm (ambient) when measurements began. The measured P_{O_2} levels in solution equilibrated gradually to the composition of the head space following each step change (Figure 3.7a). The P_{O2} measurements for wells containing cells at low densities were not statistically different from the control wells that did not contain cells. This data confirmed that oxygen measurements could be made in the presence of cells and indicated that at low cell densities, the P_{O2} levels were not affected by the cells.

When cells were plated at high densities, however, cellular consumption of oxygen lead to significant changes in solution oxygen tension (Figure 3.7b). Culture medium was again replaced at the start of the experiement (t = 0), but in this case, P_{O_2} in the presence of cells quickly dropped to a level significantly lower than that in the control well without cells (from 0.21 atm to 0.16 atm over the first 50 min). Subsequently, the P_{O2} in the cell culture responded to the step-changes in the headspace gas composition, and exhibited time constants that were similar to those observed in the low-density cultures or in the control well. However, the measured values of P_{O2} in the high-density culture remained significantly lower than that in the headspace or the measured P_{O2} in the control wells. For the confluent cell monolayer evaluated, no spatial variation in P_{O2} was

observed across the field of view (1 mm^2). Representative phase and nuclear-stained fluorescence microscopy images allowed the different cell densities evaluated here to be observed (Figure 3.7c-d). These images further demonstrated the facile integration of live-cell microscopy with this oxygen sensing strategy.

During normal metabolism in culture, cells consume oxygen continuously, and the depleted oxygen is replaced diffusively from the surrounding culture medium, the culture flask head space or the cell culture plate material. At low cell densities (Figure 3.7a) small amounts of oxygen were consumed and diffusion was sufficient to replace the consumed oxygen, giving similar results to the control. However, at higher cell densities (Figure 3.7b), the greater number of cells consumed considerably more oxygen with a significant decrease in the local oxygen concentration compared to the control. In this case, oxygen supplied by diffusion was only able to keep up with oxygen consumption once a relatively steep concentration gradient emerged between the culture substrate and the solution surface (e.g. 0.16 atm to 0.21 atm at 50 min). Once established, this gradient was maintained throughout the experiment. For example, when the headspace $P_{O2}$was brought to 0.1 atm, the measured P_{O_2} in the high density culture dropped to 0.05 atm. Without the direct measurements shown here, the local oxygen tension could only be roughly inferred by making assumptions about per-cell rates of oxygen consumption. Further, any changes in metabolic activity that affect the rate of oxygen consumption (e.g. in response to a novel drug treatment) would go unmonitored.

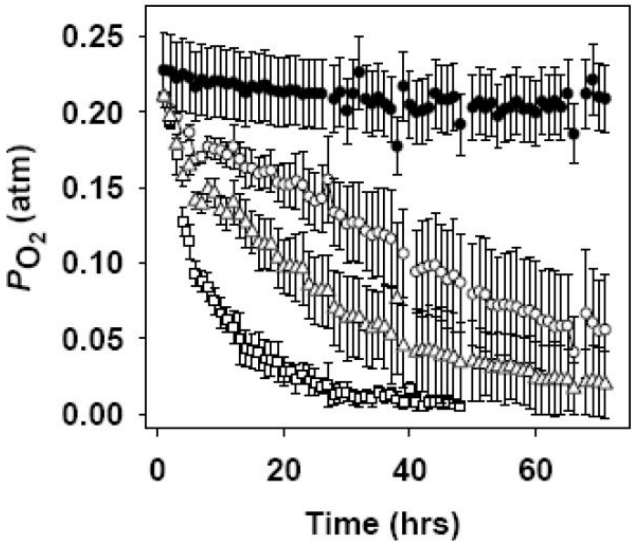

Figure 3.8 Changes in measured P_{O2} during long-term cell culture. NIH 3T3 mouse fibroblasts were seeded at three densities: 790 cells/mm^2, 1580 cells/mm^2, 3100 cells/mm^2. PtTFPP-Tef-PDMS sensors were used to measure the P_{O2} throughout three days of culture. In each case, the solution oxygen tension decreased over time relative to a control well with no cells (black circles) due to proliferation and cellular oxygen consumption. As cells proliferated over several days, oxygen tension continued to drop. Data points indicate mean P_{O2} measurements from triplicate experiments with the standard deviation shown by error bars. The difference between each seeding density was statistically significant (two factor ANOVA, $p < 0.05$).

For short observation times, the rate of oxygen consumption was constant and a stable concentration gradient was observed. However, over longer observation times, cellular proliferation increases the number of cells present as well as the rate of total oxygen consumed. These effects were observed by measuring P_{O2} immediately following the addition of suspended cells and repeating the measurement every hour for 72 h (Figure 3.8). As cells sedimented and attached to the bottom of the culture dish and then proliferated over the course of the experiment, the P_{O2} in solution decreased monotonically. Initially, between 0-8 hrs, the measured P_{O2} decreased rapidly in all cell cultures, and the steepness of the decrease correlated with the cell density. This time frame correlated with the time required for attachment of cells to the sensor surface, and

this decrease in P_{O2} was attributed to the initial formation of a stable concentration gradient between the attached cells on the sensor and the surface of the culture medium. Subsequently, P_{O2} in culture continued to drop, until it leveled off when approaching the limiting value of P_{O2} = 0 atm. The above P_{O2} response is consistent with constant cell proliferation followed by insufficient supply of oxygen by diffusion alone.

This experiment depicted the dynamic oxygen tension that can occur during long-term cell culture. For the highest cell seeding density (3100 cells/mm^2), the local oxygen tension after 24 h of culture was essentially zero. Thereafter, cell consumption of oxygen was limited by the rate of diffusion of oxygen from solution. Further, the specific oxygen tension was very dependent on the number of cells present. At the lower seeding densities (790 cells/cm^2), the oxygen level dropped throughout culture, but remained above 0.05 atm even after 72 h. The direct oxygen measurements shown here provided critical information regarding the state of the changing culture conditions throughout the long-term culture.

When P_{O2} in culture after cells attached was compared between seeding densities, it was evident that the decrease in oxygen tension correlated with the cell density in culture (Figure 3.9a). The linearity of the relationship between P_{O2} and cell density indicated that the net oxygen consumption in each case was dependent only on the total number of oxygen consuming cells. Since the cells were evenly distributed across the bottom of the well, a spatially uniform oxygen concentration gradient was assumed

between the cells and the top surface of the culture medium. The oxygen flux (J_{O2}) that resulted was analyzed using the 1-dimensional steady state solution to Fick's Law:[36,39]

$$J_{O2} = \frac{D \cdot \Delta P_{O2}}{h} \tag{3.3.2}$$

where D is the diffusivity of oxygen in aqueous solution (3.3×10^{-5} cm^2/s),[36] ΔP_{O2} is the difference in oxygen partial pressure between the cell microenvironment and the culture medium surface, and h is the height of the culture medium. Using eq 3.3.2, the P_{O2} measurements were used to calculate oxygen flux as a function of cell seeding density (Figure 3.9b). The slope of this data is the per-cell rate of oxygen consumption, and the linear relationship shows that this rate is independent of cell density for the conditions explored here. From Figure 3.9b, the per-cell rate of oxygen consumption for NIH 3T3 mouse fibroblasts is 1.38 ± 0.04 fmol·min^{-1}·cell^{-1}. This value is similar to rates of oxygen consumption reported for other cell types.[39]

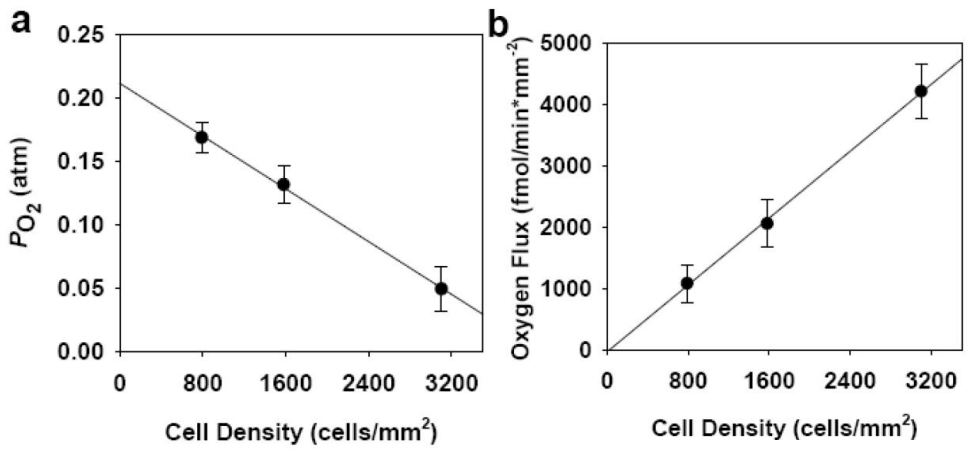

Figure 3.9 Effect of cell density on P_{O2} and oxygen consumption. Measured P_{O2} at 12 h post-seeding was plotted against the cell density (a). Fick's law was used to calculate the oxygen flux at each cell density (b). The per cell rate of oxygen consumption determined from the linear regression was 1.38 ± 0.04 fmol·min^{-1}·cell^{-1} for the NIH 3T3 mouse fibroblasts. Data points and error bars indicate the mean values and standard deviations of triplicate experiments; solid traces are linear regressions to the data.

3.4 Conclusions

We have developed a new oxygen sensor to quantify changes in oxygen tension during *in vitro* cell culture. The sensor is based on the oxygen-dependent quenching of the phosphorescent porphyrin dye, PtTFPP, which is incorporated into a gas-permeable thin polymer film. A multi-layer sensor design, with a first layer of the PtTFPP dye in PDMS, a second layer of Teflon AF, and a third (top) layer of PDMS with no dye, was found to be effective for culturing adherent cells and mitigating phototoxicity from the PtTFPP dye. A major advantage of the current thin film sensor is that it allows facile integration of oxygen measurements with both phase contrast and fluorescence microscopy to characterize and quantify cell viability, motility and cell count. Compared to previous oxygen sensors which had problems associated with photodegradation and lack of sensitivity, the current thin film sensor has high sensitivity (K_{SV} = 584 atm^{-1}) and negligible photobleaching. In situ measurements of P_{O2} during cell culture revealed significant drops in local oxygen tension for high cell densities. Further, long time cultures revealed dynamic changes in P_{O2} as cells proliferated. The rate of per-cell oxygen consumption calculated here for NIH 3T3 fibroblasts was consistent with reported values for other cell types. The method reported here to measure oxygen tension *in situ* during cell culture will enable the effects of local oxygen levels on cell behavior to be determined and provide the needed measurements for controlling this important component of the cellular microenvironment.

Chapter 4

Oxygen Measurements in Hepatocyte Culture

4.1 Introduction

The liver functions as the central organ for xenobiotic metabolism and is responsible for modification, clearance and potential toxicity effects that arise from drug intake. Unforeseen drug induced liver toxicity is one of the major causes of post market drug withdrawal.[51,52] As such, identifying hepatotoxicty prior to clinical phases or market entry is critical given the high cost associated with drug development.[53] *In vitro* cultures of hepatocytes are a widely accepted model for testing and determining liver toxicity.[54] However, many reports have shown that hepatytoces (primary) lose their liver-like functions in conventional cultures[54]. Therefore, precise regulation of culture parameters to preserve the proper hepatic phenotype has wide implications for predicting the response of liver cells to drugs.

In mammalian cell cultures, oxygen levels have been shown to affect growth, differentiation and cell functions. During respiration, oxygen is the key electron acceptor at the end of the electron transport chain facilitating efficient generation of ATP. Due to their high metabolic activities, oxygen consumption rates for hepatocytes are significantly higher (an order of magnitude) than other cell types.[55] As such, the oxygen levels and the supply of oxygen are critical to hepatocyte functions. *In vivo*, the blood

supply to the liver is distributed heterogeneously and hepatocytes are exposed to a range of oxygen levels from the periportal to the perivenous regions.[56] The oxygen levels induce hepatocytes to express different enzymes, thus creating zones with distinct metabolic functions across the liver. Such "zonal" property has been demonstrated *in vitro* by adjusting the oxygen level in a flat-plate perfusion system and by controlling the medium height to simulate different oxygen conditions in static cultures.[27,57] While low oxygen levels appears to facilitate the induction of certain cytochrome P450 expressions, hepatocytes in general demand sufficient oxygen supply to maintain proper metabolic functions. In freshly seeded hepatocytes, oxygen measurements revealed a 300% increase in oxygen utilization rate, demonstrating the high demand for oxygen during the transition from suspended cells to attached cells.[55] Rotem el al. found that hepatocytes increased cell attachment and spreading area as a result of increasing oxygen level supplied to the culture.[58] In addition, co-cultures of hepatocytes under elevated oxygen conditions showed higher levels of metabolic activity compared to those under ambient oxygen level.[59,60] These findings demonstrate that hepatocytes are extremely sensitive to their surrounding oxygen level and proper monitoring of oxygen environment is critical.

In conventional static 2-dimensional culture where cells are seeded at the bottom of multiwell dishes, oxygen is supplied by passive diffusion through a height of culture medium. Due to the low solubility of oxygen and the diffusion barrier created by the liquid, an oxygen gradient is formed as a result of cellular respiration at the bottom of the dish (Figure 4.1).[61] If oxygen levels are not properly monitored, depletion of oxygen could result in hypoxia leading to unintended hypoxia-induced changes in cell behavior.

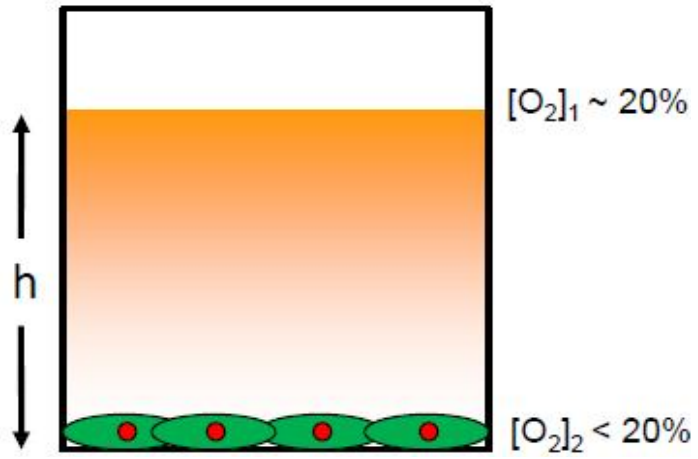

Figure 4.1 Conventional 2D format of cell culture. Schematic illustrates cells adhered to the bottom of the well are exposed to lower oxygen level compared to the head space above media as a result of oxygen consumption and the diffusion barrier created by height of the liquid above cells.

In the following study, cells from a human hepatocellular carcinoma cell line, HepG2, were cultured in a multiwell dish incorporated with the planar oxygen sensor previously developed in Chapter 3. The sensor, based on oxygen quenching of a phosphorescent molecule, allowed non-invasive real time oxygen measurements to be made. Continuous oxygen measurements revealed the cells in culture were unexpectedly exposed to hypoxic conditions and the per-cell oxygen consumption rate confirmed the high oxygen demand of these cells. Oxygen fluxes (a measure of oxygen consumption rate) of HepG2 cultures increased asymptotically reaching a plateau at high densities. This phenomenon was attributed to the insufficient oxygenation at these densities. In addition, oxygen levels within HepG2 cell clusters were measured and the results showed unique distribution of oxygen levels across the clusters.

4.2 Experimental Methods

Cell Culture. Human hepatocellular carcinoma cell line HepG2 (ATCC, Manassas VA) were cultured in Eagle's Minimum Essential Medium (MEM; Mediatech, Herndoon, VA) supplemented with 10% (v/v) fetal bovine serum in a T-25 polystyrene flask. Cells were maintained in humidified air balanced with 5% (v/v) CO_2 under 37^{o}C. Cells were kept in the incubator and medium was changed every 2 days until experiments began.

Sensor Preparation. Multilayer oxygen sensor was prepared as previously described.[62] Briefly, Pt(II) *meso*-tetrakis(pentafluorphenyl)porphine (PtTFPP, Frontier Scientific Inc., Logan, Utah) was mixed with poly(dimethylsiloxane) (PDMS, Sylgard 184; Dow Corning, Midland, MI) and spin-coated onto 12 mm glass cover slips. Upon curing, a thin film of Teflon AF (Dow Chemical) was spin-coated on top of the previous film followed by a final film of PDMS layer without dye with the final sensor thickness of approximately 25 μm. The sensor was bonded into a 24-well plate with 0.5 μL of PDMS. Prior to cell seeding, bovine fibronectin solution diluted in PBS (25 μg/mL) was added to the sensor for 1 hr to facilitate cell attachment. The fibronectin solution was aspirated out and suspended cells were added directly onto the fibronectin-coated sensor.

Continuous Oxygen Measurement in Culture. HepG2 cells were seeded on top of the oxygen sensors under 2.5 mm or 5 mm of culture medium. Six seeding densities were examined (75 cells/mm^2, 150 cells/mm^2, 300 cells/mm^2, 600 cells/mm^2, 1200 cells/mm^2, and 2400 cells/mm^2). Upon seeding, cells were immediately placed on an inverted Axiovert Z1 microscope (Zeiss, Thornwood, NJ) with an automated staged and kept

under 37°C with a microscope attached incubation system. The culture headspace was kept under humidified gas containing 5% CO_2 and 20% O_2 supplemented with N_2. Image recording began immediately afterwards.

Western Blotting. HIF-1α expressions were quantified by immunoblotting. Four separate HepG2 culture conditions were prepared and examined. Cells were seeded at 150 cells/mm^2 with 2 mm of culture medium and kept in either 1.) 20% O_2, 2.) 1% O_2, or 3.) with 1.5 μM $CoCl_2$. The fourth condition consisted of cells at 300 cells/mm^2 under 5 mm of medium. After 24 hrs in each conditions, cells were rinsed with ice-cold PBS and lysed with chilled SDS-PAGE Sample Buffer (Biorad, Hercules, CA) using a cell scrapper. Cell lysates were collected and immediately boiled at 95°C for 5 minutes and then kept on ice. Protein separations from lysate were performed on 4-20% (w/v) gradient polyacrylamide gels (Biorad) and transferred onto PVDF membranes. A 3% (w/v) BSA in PBS was used to block the membranes. Membranes were then probed with a 1:5000 dilution of mouse anti-human HIF-1α monoclonal antibody (Becton Dickinson, San Diego, CA) in blocker solution. Chemiluminescence detection was used along with horse radish peroxidase-labeled secondary antibody to detect the bands on the membrane. A Genegnome Imager (Syngene, Frederick, MD) was used to image the bands for further analysis. Band intensities were normalized with total actin using an actin antibody (Sigma, St Louis, MO).

4.3 Results and Discussion

During normal respiration, cells consume oxygen and thereby alter their surrounding oxygen environment. In the current study, oxygen measurements were made continuously for 24 h upon seeding HepG2 cells under 5 mm of culture medium. The measured oxygen levels in these cultures showed an immediate drop followed by a steady decrease throughout the experiment (Figure 4.2). The significant decline in oxygen levels during the initial period of the culture has been suggested as a result of the high energy demand required by cells to facilitate attachment and spreading,[55] as observed in primary hepatocyte cultures. In addition, the drop in oxygen levels becomes greater as the seeding density increases, demonstrating the impact of cell number on cellular oxygen levels.

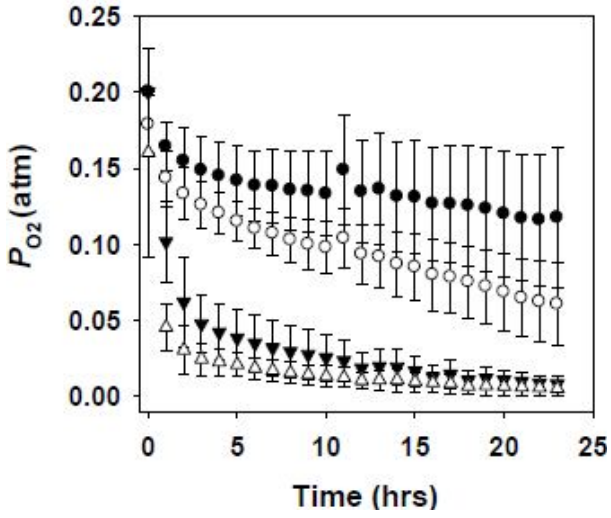

Figure 4.2 Oxygen level changes in hepatocyte culture. HepG2 were cultured under 5 mm of culture medium and seeded at 6 different densities. Representative densities are shown: 75 cells/mm^2 (black circle), 150 cells/mm^2 (white circle), 600 cells/mm^2 (black triangle), and 1200 cells/mm^2 (white triangle). Oxygen sensor measurements showed oxygen level decreased over time in HepG2 culture as a result of oxygen consumption by the cells. Increases in cell density resulted in faster decreases in oxygen level. Data and error bars represent mean values and standard deviations from triplicate experiments.

HepG2 cultures are highly metabolically active and therefore the oxygen levels in these cultures decreased sharply within 24 h of seeding. For high density cultures (1200 cells/mm^2), cells were exposed to a hypoxic environment within 2 h after seeding. Even for low seeding density cultures (150 cells/mm^2), the oxygen environment around HepG2 decreased well below partial pressures of oxygen (P_{O2}) of 0.1 atm within 24 h, demonstrating the high oxygen demand by these cell lines.

To quantify the changes of oxygen flux as a result of seeding density, the steady state solution of Fick's law was applied,[36,39]

$$J_{O_2} = \frac{D\Delta P_{O_2}}{h} \tag{4.3.1}$$

where J_{O2} is the flux, D is the diffusion coefficient of oxygen in water, ΔP_{O2} is the difference of the partial pressure of oxygen between the air-liquid interface and the cell layer, h is the height of culture medium above cells. At t = 12 h, low seeding density cultures ($\leq$ 300 cells/mm^2) demonstrated oxygen fluxes that increased linearly with cell density, resulting in a per-cell oxygen consumption rate of 29 ± 6 fmol·min^{-1}cell^{-1} for HepG2, consistent with previously reported literature values for hepatocytes (Figure 4.3).[55] However, as the density increases, the oxygen flux leveled off, reaching the theoretical maximum of the culture. This theoretical maximum of oxygen flux was calculated by setting the maximum difference in the oxygen level between the boundary conditions. By reducing the liquid height (h) above HepG2 to 2.5 mm, the diffusion barrier for oxygen was decreased. The linear correlation between oxygen flux and seeding density was once again observed at low densities. At high densities ($\geq$ 600 cells/mm^2) the fluxes increased substantially compared to cells grown under 5 mm of

culture medium and the values plateaued towards a higher maximum flux calculated based on the new geometry (Figure 4.3).

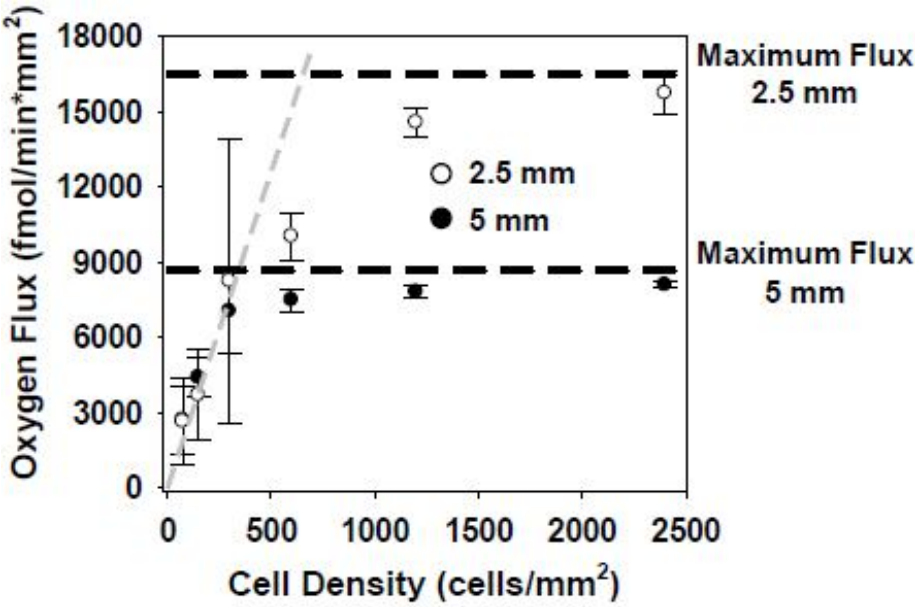

Figure 4.3 Height of culture media impacts oxygen consumption. P_{O2} measurements of HepG2 culture were measured at 12 hr post seeding for cultures with 2.5 mm and 5 mm of culture media. Steady-state Fick's law was applied to calculate the change of flux as a result of cell density. Linear regression performed on low density culture revealed that the per-cell oxygen consumption rate for HepG2 was 29 ± 6 fmol/min^{-1}·cell^{-1}. Dashed lines (black) represent the theoretical maximum flux for the cultures. Data points and error bars are the means and standard deviations from 3 separate experiments.

In a conventional static culture, passive diffusion of oxygen through the culture medium provides the primary means of oxygenation for adherent cells. When sufficient amounts of oxygen are provided, the oxygen flux increased linearly with cell density resulting in a constant per-cell oxygen consumption rate (Figure 4.3). In contrast, when oxygen diffusion was the limiting factor, the linear correlation no longer applied and the fluxes reached a maximum at high densities. At first glance this appears to suggest that oxygen consumption rate for HepG2 is density dependent. However, by decreasing the

oxygen diffusion barrier (increasing the oxygen supply) the fluxes increased substantially. This suggests the apparent decrease in oxygen consumption rate is a direct result of the inadequate supply of oxygen, thus limiting the amount of oxygen that can be consumed. When more oxygen is available, the oxygen consumption rate increases. Contrary to previous reports that suggest hepatocytes lower their oxygen consumption rate at high densities, the results shown here imply that the decrease is an artifact of inadequate oxygen supply and cells will resume to their basal levels of oxygen consumption when sufficient oxygen is present.

In contrast to other cells lines, HepG2 cells have an epithelial morphology and adhere strongly to their neighboring cells. As such, cell clusters formed spontaneously during culture (Figure 4.4a). Unlike monolayer cultures that adhere uniformly across a surface, these clusters typically contain a high density of cells aggregating into multiple layers that result in a densely populated, 3-dimensional structure. As the clusters consume oxygen, the surrounding oxygen environment changed, which resulted in variations in sensor intensity (Figure 4.4b). Upon conversion into oxygen levels, the results showed localized variations of oxygen tensions that directly overlapped with the location of cell clusters (Figure 4.4c). In addition, oxygen gradients can be clearly visualized across these cell clusters where oxygen level is the lowest at the center and then rises towards the edges (Figure 4.4d-e). The observed effects could be attributed to the high density of the cells in the middle of the clusters, thereby creating an oxygen sink observed by the underlying sensor.

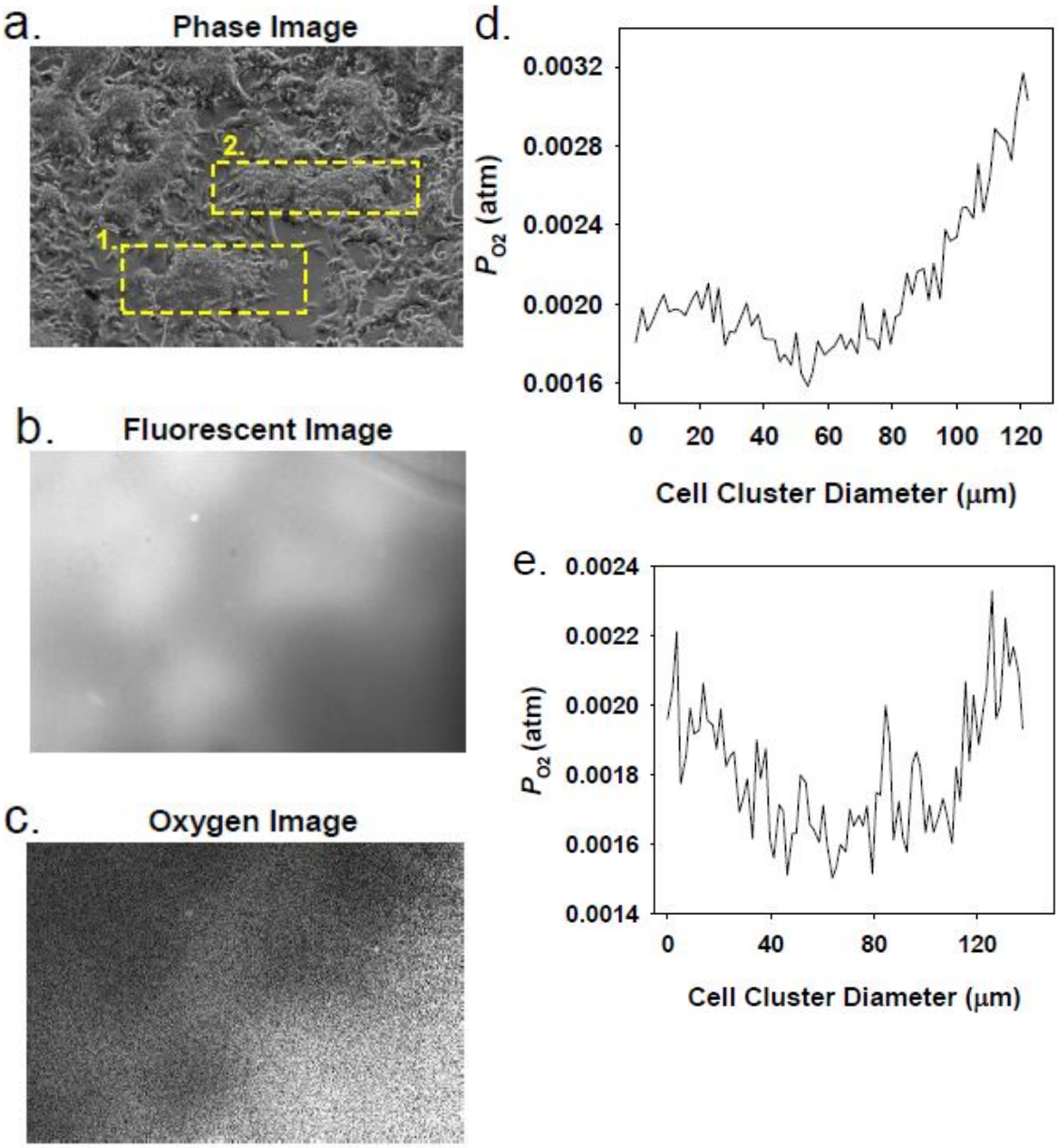

Figure 4.4 Oxygen level in HepG2 cell clusters. During culture, HepG2 cells form cell clusters as shown by the phase contrast image (a). Fluorescence from the oxygen sensor showed localized changes of intensity that corresponded to the location of the clusters (b). False-color oxygen image confirmed the localized changes of oxygen levels due to the cell clusters (c). Small oxygen gradient were observed from the edge to the center of cell clusters 1 and 2 in (d) and (e).

The transcription factor, hypoxia-inducible factor 1 (HIF-1), plays a central role in regulating oxygen homeostasis. HIF-1 is a heterodimer with a α subunit (HIF-1α) and a β subunit (HIF-1β); where the β subunit is constitutively expressed in the nucleus while the α subunit expression is subject to the surrounding oxygen levels.[7,63] In the presence of the oxygen, HIF-1α is subject to hydroxylation which leads to proteolysis and degradation. Under hypoxic conditions, hydroxylation processes are suppressed and HIF-1α expression is stabilized and binds to the β subunit, thus forming an active transcription factor that leads to regulation of genes involved in angiogensis, metabolism, growth and apoptosis.[7,64]

HIF-1α expressions in HepG2 were quantified via western blotting to determine the biological responses to the changing oxygen environment during culture. Using Figure 4.2, cell densities and medium height were selected to create hypoxic and non-hypoxic cultures after 24 hrs. Surprisingly, HIF-1α expressions were not statistically different amongst the different culture conditions despite the results of oxygen measurement (Figure 4.5). Only cultures treated with 1.5 μM $CoCl_2$, which chemically induces hypoxia-like response,[65,66] demonstrated significant increases in HIF-1α expressions. Interestingly, even cells cultured under hypoxia (P_{O2} of 0.01 atm) demonstrated statistically lower HIF-1α compared to that after $CoCl_2$ treatment. Further studies will be needed to elucidate the lack of HIF upregulation.

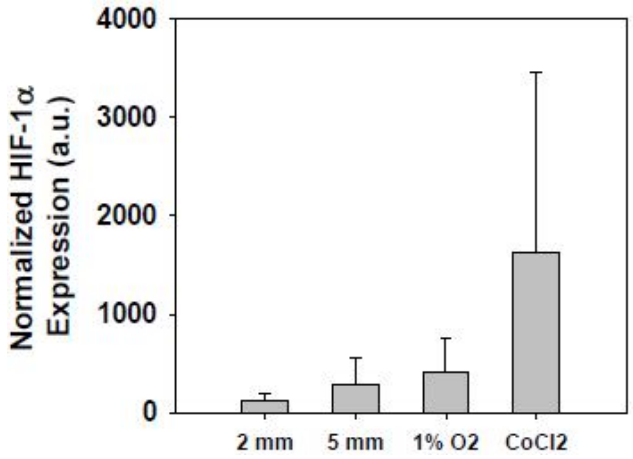

Figure 4.5 HIF-1α expression in HepG2 cells under different culture condition. Western blot analysis revealed no statistical differences in HIF-1α expression under hypoxic (1% O2 and 5 mm) and non-hypoxic (2 mm) conditions. In contrast, HepG2 cultured with 1.5 μM of $CoCl_2$ showed significantly higher expression of HIF-1α compared to the other cultures. Data were normalized against actin expression.

4.4 Conclusions

In the current study, continuous oxygen measurements of HepG2 cultures were performed using a non-invasive oxygen sensor. Due to the high oxygen consumption rate of HepG2 cells, oxygen measurements demonstrated that cells were exposed to hypoxic conditions within 24 h after seeding. Oxygen flux calculations showed that the decrease in oxygen consumption rate at high densities reported in previous reports could be attributed to the lack of sufficient oxygen supply: when more oxygen was supplied to the cells (reducing medium height), the per-cell oxygen flux appeared to increase. In routine culture, HepG2 cells attach to their neighboring cells and form clusters. The oxygen sensor revealed that oxygen gradients existed across these cell clusters, and such findings could have implications for other cell types that form clusters or cell aggregates,

including stem cells and cancer cell lines. Interestingly, HIF-1α expression in HepG2 cultures exposed to hypoxic conditions was statistically indistinguishable from that in well-oxygenated cultures. This finding is peculiar since low oxygen levels typically cause stabilization and upregulation of HIF-1α expression. Future studies will further examine the causes for the lack of differences in expression.

Chapter 5

Oxygen Measurements in Microfluidic Systems

5.1 Introduction

Oxygen is a critical parameter for cell survival and homeostasis. While oxygen is required for ATP production, too much or too little oxygen greatly changes cell response and behavior. In vitro studies have demonstrated that oxygen levels affect cellular growth[67], enzyme expression[57] and stem cell differentiation[68,69]. Also, oxygen gradients as a result of mass-transfer limitations occur naturally in normal and developing tissues as well as within growing tumour masses. These oxygen gradients have been suggested to regulate proper tissue function[70], influence cell development[69], and elicit the onset of angiogensis[71]. To improve our understanding of oxygen-dependent cellular behavior, proper control of oxygen level during cell culture is critical.

In general, mammalian cells in tissue are found at an oxygen partial pressure (P_{O2}) of 3% to 9% oxygen (P_{O2} = 0.03 atm – 0.09 atm).[35] In contrast, in conventional cell culture, cells are maintained at the ambient level of 21% oxygen (P_{O2} = 0.21 atm). To reduce the oxygen level during *in vitro* cell culture, various hypoxic chambers have been utilized.[72,73] However, the time required for culture medium to reach equilibrium and the lack of ability to generate oxygen gradients limit the scope of application for such chambers.[74]

Gas-permeable poly(dimethylsiloxane) (PDMS)-based microfluidic devices offer alternative approachs to existing methods of oxygen regulation.[31,75-79] Utilizing passive diffusion, external oxygen gas pumped through a control channel equilibrates through PDMS with the dissolved oxygen in adjacent fluidic channels, thereby achieving oxygen regulation on the device. Given the small distance between channels and the high permeability of oxygen through PDMS, equilibrium can be achieved quickly (within seconds).[78,79] In addition, oxygen gradients can be generated using different oxygen-nitrogen gas mixtures across a device.[79] While this method of oxygen control is an improvement, the current design allows significant pervaporation of water through the PDMS.[80] In mammalian cultures where the temperature is held at 37°C, the aqueous liquid within a fluidic chamber can quickly evaporate and pass through the PDMS, resulting in dramatically increased osmolarity of the liquid. This issue is potentially exacerbated when gas-filled control channels are placed in close proximity to fluidic channels for gas control. To circumvent this problem, mammalian cells are often cultured in the device under continuous flow conditions. However, this precludes culturing cells that are sensitive to shear stress and limits the potential applicabilty of microfluidic methods.

In the current study, we demonstrate a new approach to regulating oxygen on a microfluidic chip. In contrast to previous methods, oxygen levels in stagnant on-chip chambers here were modulated by moving aqueous solutions with different dissolved oxygen levels through neighboring control channels. Utilizing an off-chip gas exchanger, the control solutions are first equilibrated with the gas in the gas exchanger and

subsequently flowed through the device. We demonstrate that this method can effectively regulate the oxygen level and also significantly reduces the effect of pervaporation. In addition, we use an oxygen sensor[62] integrated into the PDMS device to monitor the changing oxygen level within the fluidic chamber continuously and in real-time.

5.2 Experimental Methods

PDMS-based multilayer microfluidic devices were fabricated using photolithography and soft lithography techniques.[81] The current design has a single fluidic line that flows into a cell culture chamber, which is positioned between two control lines (Figure 5.1). Pneumatic valves were placed upstream and downstream from the culture chamber to regulate the liquid flow. Control lines and the culture chamber were 250 μm and 1000 μm wide, respectively. Two designs were tested: in one, the horizontal distance between the culture chamber and the control line was 200 μm and in the other this distance was 80 μm. The vertical distance between the two was ~ 10 μm in all cases. All channels were 30 μm tall. The gas exchanger was constructed using gas-permeable Teflon AF tubing with i.d. = 600 μm and o.d. = 800 μm (Biogeneral Inc, San Diego, CA).

An oxygen-sensing PDMS film, based on the porphyrin dye, Pt(II) meso-tetrakis(pentafluorophenyl) porphine (PtTFPP, Frontier Scientific Inc, Logan, Utah), was prepared and calibrated as described previously.[62] Briefly, PtTFPP was dissolved in PDMS (Slygard 184; Dow-Corning, Midland, MI) and spin coated onto a microscope slide. Separate layers of Teflon AF (Dow Chemical) and PDMS were

sequentially spin-coated and cured. The total sensor thickness was ~ 24 μm. This oxygen sensor was integrated with the microfluidic device through plasma bonding. Calibration of the on-chip sensor was accomplished by exposing the device to different oxygen levels. Emission intensity from the sensor was captured and used to generate a calibration curve. Because the thin-film sensor covered the whole device, spatial variations in oxygen level could be monitored across the entire deivce.

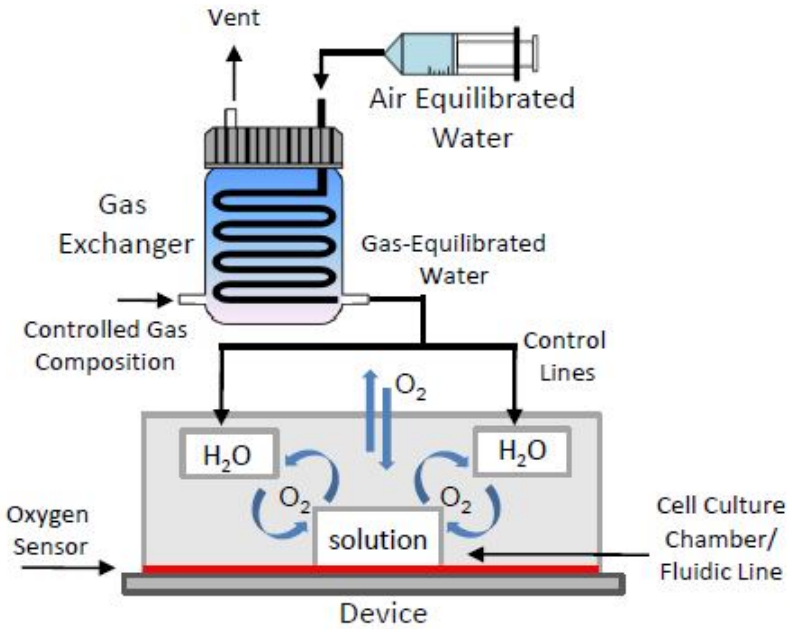

Figure 5.1 Schematic of microfluidic device setup for on-chip oxygen regulation. Water is pumped through the gas exchanger where the P_{O2} in the liquid is reduced via equilibration with the controlled gas composition. This solution then enters the control lines flanking cell chamber of the device. Oxygen sensor integrated with the device (red) measures changes of P_{O2} as dissolved oxygen in the control lines diffuse through the PDMS and into the adjacent cell chamber. Schematic not drawn to scale.

Pervaporation experiments were performed at a temperature of 37°C. A 10 μM solution of dextran conjugated with rhodamine (molecular weight ~70,000; Sigma, St. Louis, MO) was used as a marker for changes in the solute concentration. A steady-state 2D finite element model was developed using FlexPDE software based on the

the device and channel geometry (Figure 5.2).

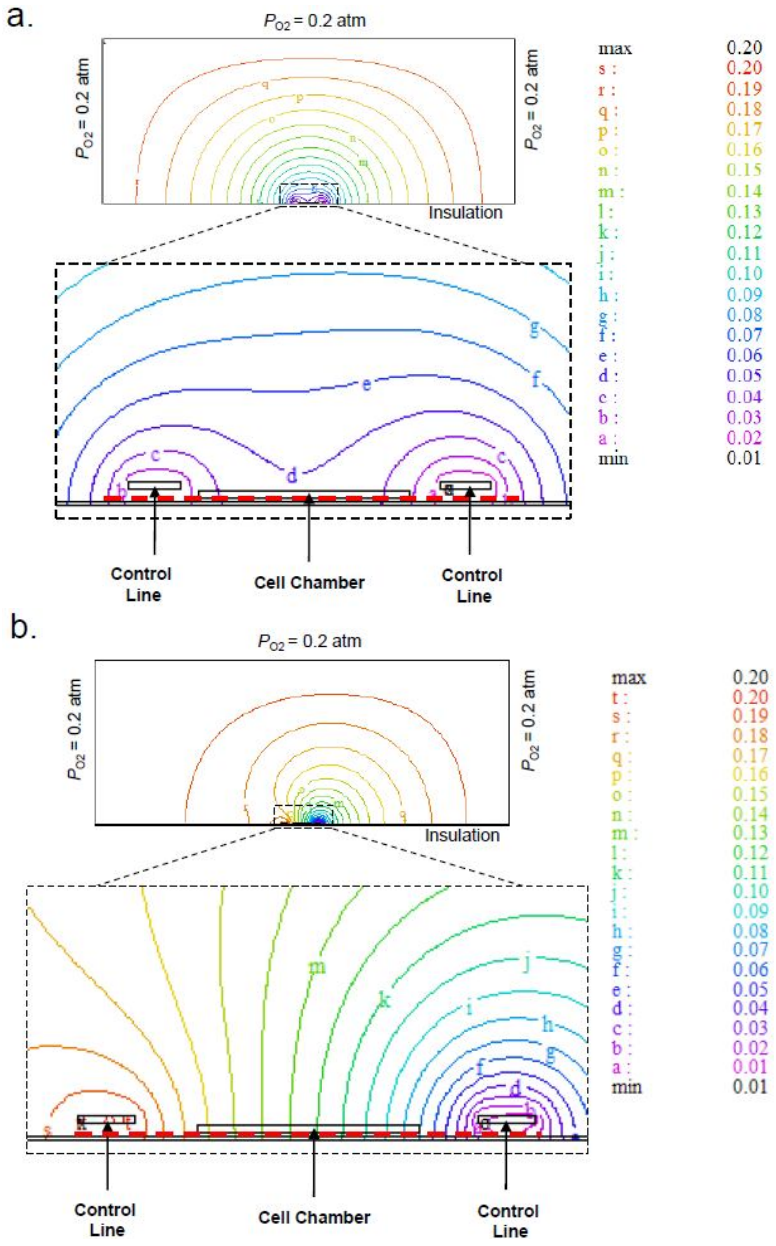

Figure 5.2 Two dimensional steady state numerical simulation of oxygen levels in a microfluidic device. The simulated geometry was 21 mm wide x 8 mm high, with boundary conditions of P_{O2} = 0.2 atm on three sides exposed and an oxygen impermeable bottom. The legend provides the P_{O2} (in atm) of the contour lines. When the boundary conditions of the two control lines were set at P_{O2} = 0.02 atm (left) and 0.012 atm (right) to match the sensor measurements, oxygen level on-chip was reduced (a). The inset shows the two control lines flanking the cell chamber and the location of simulated oxygen measurement (red dashed line). To simulate oxygen gradient, P_{O2} of control lines were set at 0.2 atm (left) and 0.008 atm (right) based on the experimental measurements (b). The current simulation consists of 60536 nodes.

5.3 Results and Discussion

Regulation of oxygen level on-chip was accomplished using an off-chip gas exchanger. Water, pumped through the gas exchanger, first equilibrated with the oxygen level there. The high oxygen permeability of Teflon tubing (990 barrer, from manufacturer website) and the short diffusion distance (tubing wall thickness ~ 100 μm) allowed rapid equilibration with the P_{O2} set point. At a flow rate of 700 μL/min (residence time of the liquid in the gas exchanger was ~100 s), the oxygen level in the liquid had fully equilibrated by the time the liquid left the gas exchanger.

Previously, we had developed a PDMS-based, thin-film oxygen sensor using the phosphorescent dye, PtTFPP.[62] Here, we integrated this sensor film into the floor of the microfluidic device through plasma bonding. The emission intensity from the film is quenched in the presence of oxygen, and the relationship between the two is given by the linear Stern-Volmer equation:[12]

$$\frac{I_0}{I} = 1 + K_{SV} \cdot [P_{O2}] \tag{5.3.1}$$

where I_0 is the phosphorescence intensity of the sensor under pure N_2 (P_{O2} = 0 atm), I is the quenched intensity at elevated oxygen levels, K_{SV} is the Stern-Volmer constant and P_{O2} is the partial pressure of oxygen. The calibration of the sensor was performed via pixel-by-pixel analysis where each pixel was assigned a separate Stern-Volmer constant. The K_{SV} determined for the on-chip sensor (517 atm ± 100 atm) matched previous bulk sensors[62], indicating that the sensitivity of the measurement was not affected by the assembled microfluidic device (Figure 5.3). As liquid carrying lower

dissolved oxygen was introduced on-chip, the oxygen level within the device equilibrated by diffusion and was detected by the oxygen sensor.

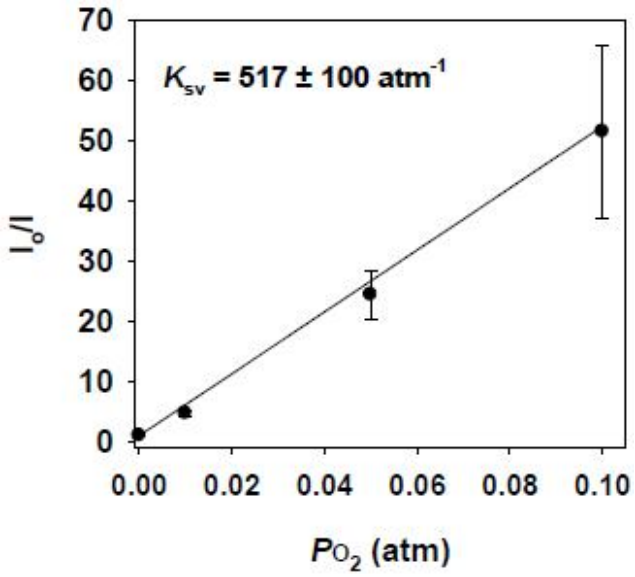

Figure 5.3 On-chip P_{O2} sensor calibration. The response of the integrated oxygen sensor follows the Stern-Volmer equation. Data points represents the mean value of all the pixels (360000 pixels) and error bars indicate their standard deviation.

Given the small volume of liquid within the microfluidic device, pervaporation can rapidly alter solute concentrations, potentially affecting a cell culture experiment. To monitor the changes in solute concentration during operation, emission intensity of dextran conjugated with rhodamine was monitored continuously in the fluidic channel while a downstream valve was closed. When warm humidified air was pumped through the control lines, an increase in rhodamine fluorescence with time was observed in the stagnant fluidic channel (Figure 5.4a). This was consistent with fresh rhodamine solution entering the chamber to replace liquid lost through pervaporation. From the steady increase in solute concentration, an osmolality doubling time of 2 h was calculated. For the geometry of the system, this gave a pervaporation rate of ~0.25 nL/min. In contrast,

pervaporation effects were minimized when warm liquid was pumped through the control lines, and no increases in rhodamine intensity were observed (Figure 5.4b). The use of water-filled control lines here is analogous to the incorporation of a water reservoir on the device to prevent pervaporation.[82]

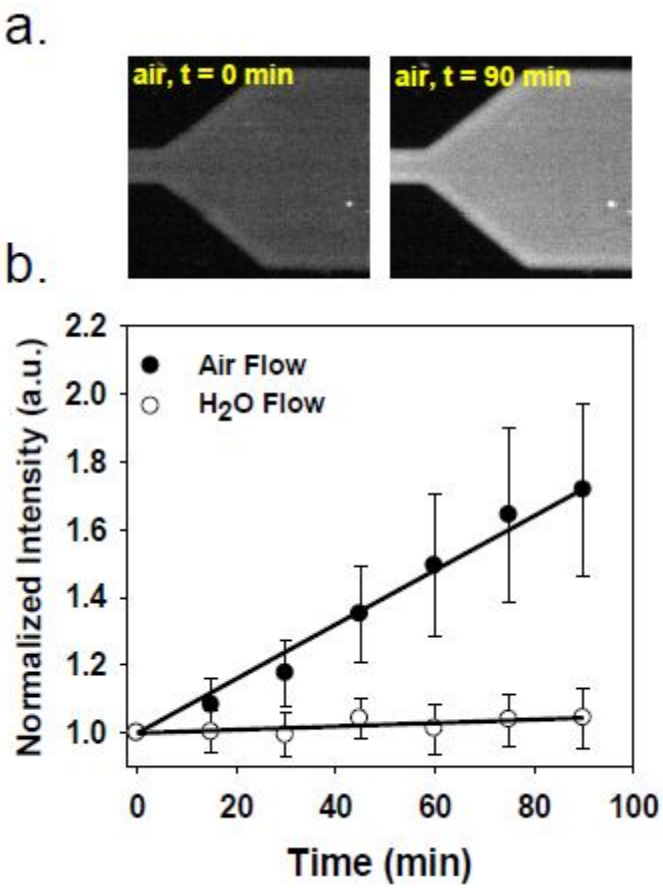

Figure 5.4 Effects of water pervaporation during device operation. Fluorescent intensity of dextran conjugated rhodamine solution increased due to pervaporation when humidified air was pumped through the control lines (a). On-chip regulation of gas partial pressure using water-filled control lines (white circle) mitigated the effects of pervaporation as compared to humidified gas flow (black circle) (b). A pervaporation rate of 0.248 nL/min was determined from calculation based humidified using d gas flow and the device geometry. Pervaporation experiment were performed at 37°C. Data points represent normalized mean intensity value across the cell chamber (triplicates) with standard deviation indicated by error bars. Solid lines show the linear regression for each system.

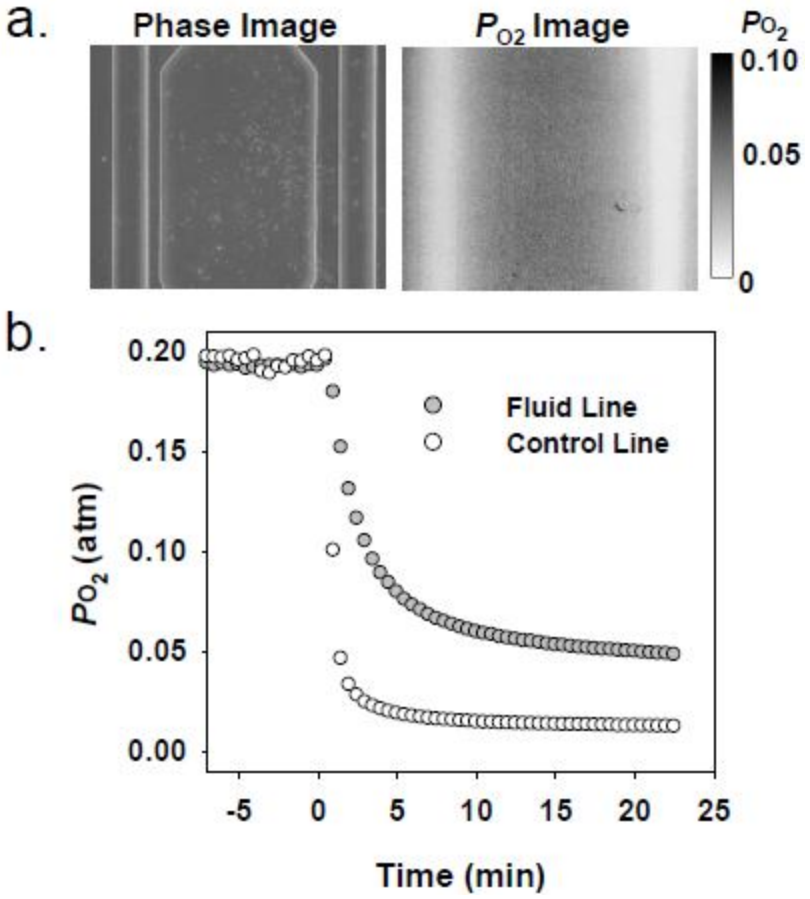

Figure 5.5 Rapid P_{O2} response on-chip. Phase contrast (left) and P_{O2} (right) images of the microfluidic device show the position of cell chamber with two flanking control lines (a). Initially, water equilibrated with air (from the gas exchanger) flows through the control lines, And the P_{O2} in the stagnant fluid chamber remains at 0.2 atm. When air is switched to N_2 (P_{O2} = 0.2 atm; t = 0 min), the oxygen level in the control line reaches steady state within 2 min, matching closely the residence time of liquid in the gas exchanger (b). Steady state oxygen level in the fluid line is achieved in 8.5 minutes. The P_{O2} image is taken from t = 20 min in (b).

By reducing the P_{O2} in the control lines, oxygen levels can be reduced across the fluid channel. The thin film sensor integrated into the floor of the microfluidic system allowed spatial variations in P_{O2} across the entire device to be monitored (Figure 5.5a). Previous devices demonstrated oxygen regulation by directly overlapping the gas and fluid channels. Adler et al. demonstrated the ability to

generate different oxygen gradients by designing multiple control lines directly above a liquid line.[79] Equilibration times in these systems varied depending on the distance between channels, and were typically on the order of seconds. The current device minimizes potential light scattering and optical interference by incorporating control lines adjacent to the fluidic chamber.

With the current system, steady state in the control lines was achieved in 2 min after air was switched to N_2 in the gas exchanger (Figure 5.5b). The oxygen level in the fluid line equilibrated more slowly and reached a steady state in 8 min. A P_{O2} across the whole device of 0.03 to 0.05 atm was achieved with this design (Figure 5.6a), providing a physiologically relevant oxygen enviornment. A 2D finite element model was developed based on the steady state diffusion equation:

$$D_{O2}\frac{\partial^2 C}{\partial x^2} = 0 \tag{5.3.2}$$

where D_{O2} is the diffusion coefficient of oxygen in PDMS, c is the oxygen partial pressure and x is the distance. Based on the cross section of the device, simulations were performed to determine the on-chip oxygen level as solutions with different dissovled oxygen content were pumped through the control lines (Figure 5.2). The simulation showed good agreement with the experimental data (Figure 5.6a) indicating oxygen transport in the device can be explained with a simple 2D diffusion model from eqn (5.3.2).

By pumping air-equilibrated and N_2-equilibrated water into opposing control lines, an oxygen gradient was formed across the device (Figure 5.6b). The finite

element model again showed good agreement with experimental data.

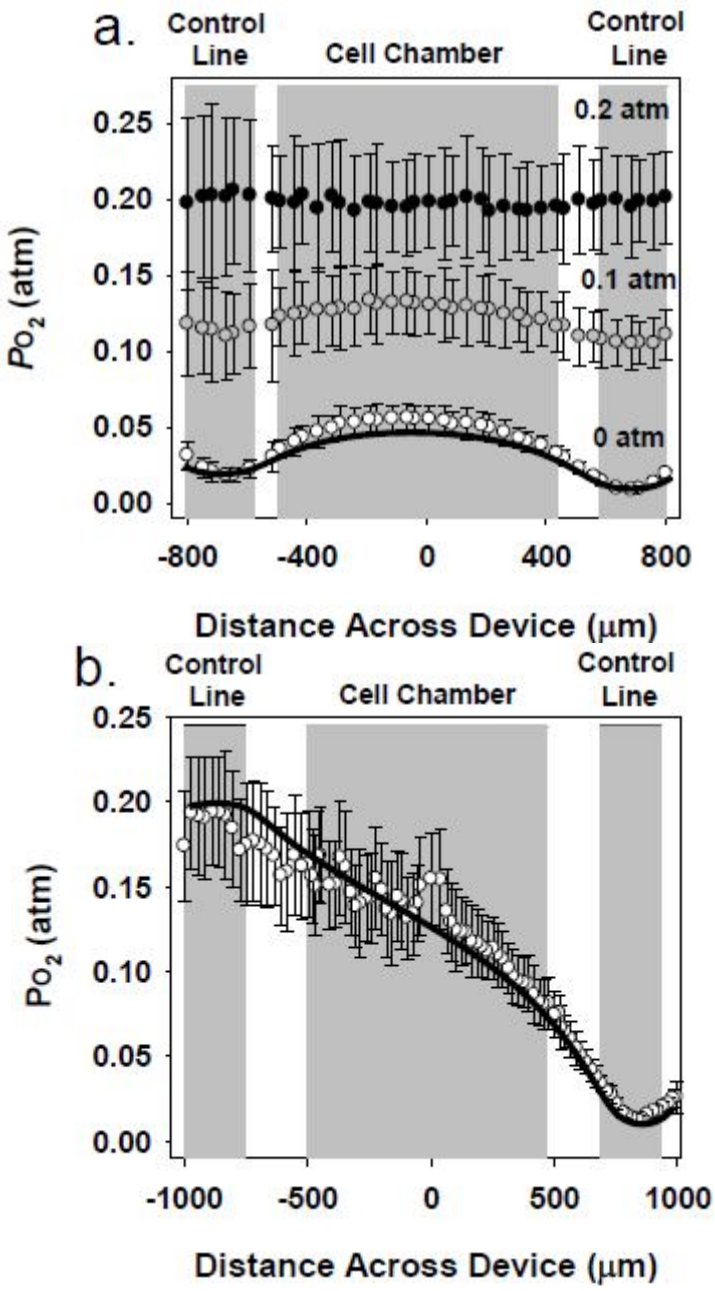

Figure 5.6 P_{O2} equilibration. The oxygen level across the device equilibrated with various P_{O2} set points in the solutions pumped through the control lines (a). By flowing air equilibrated and N_2 equilibrated water on opposite sides of the cell chamber, an oxygen gradient was formed across the device (b). Oxygen measurements from the sensor match the result of a finite element simulation (black line). Grey regions in the graphs indicate the location of the two control lines flanking the middle cell chamber, separated by PDMS membrane in white. Data points represent the mean P_{O2} value with standard error shown with error bars.

5.4 Conclusions

Precise regulation of oxygen level during cell culture is critical to understanding how oxygen affects cell function and response. Gas permeable PDMS based microfluidic devices offers the advantage of fast and precise control of oxygen level. However, continuous operation can result in pervaporation and dramatic changes in solute concentration that negatively affect cell behavior. We have developed a microfluidic cell culture system that accurately measures and controls oxygen level while mitigating pervaporation. An oxygen sensor, integrated into the floor of the microfluidic device allows real time monitoring of oxygen level on-chip. Instead of pumping gas through the device, liquids with varying oxygen concentrations, controlled with an off-chip gas exchanger, were pushed through the control lines to achieve regulation of oxygen level. We demonstrated that physiological oxygen levels (P_{O2} of 0.03 atm to 0.05 atm) can be maintained on-chip. Oxygen gradients were also generated. Experimental P_{O2} measurements showed excellent agreement with a finite element simulation. The current strategy allows the oxygen level to be monitored across the entire device, thus providing a tool for understanding how changes in oxygen level propogates throughout the entire microfluidic system.

Chapter 6

Conclusions and Recommendations

6.1 Conclusions

Oxygen is a critical component to cell surivial and a key modulator affecting cell viability, growth, and differentiation. *In vivo,* cells are typically found within 200 μm of blood vessels and capillaries but are exposed to a wide range of oxygen levels and gradients that are tissue dependent. It is critical *in vivo* to maintain a proper balance between oxygen delivery and oxygen consumption by the cells. In contrast, conventional cell cultures are routinely performed under atmospheric levels where the cells receive oxygen supply via passive diffusion through millimeter distances of culture medium. This exposes cells to non-physiological oxygen levels, potentially creating hypoxic conditions during culture and ultimately affecting cell behaviors and responses. In this dissertation, we have reported the development of a new oxygen sensor for cell culture based oxygen measurements.

The sensor was prepared by incorporating the phosphorescent dye platinum porphyrin (PtTFPP) into gas permeable PDMS thin films (Chapter 3). Based on the oxygen-dependent quenching of dye emission, non-invasive oxygen measurements were made in real time. Through proper selection of components, the resulting oxygen sensor

demonstrated an order of magnitude higher sensitivity compared to previous sensors. The multilayer design provided a suitable substrate for cell attachment and mitigated against toxicity effects. During long term cultures of NIH 3T3 fibroblasts, the sensor exposed the dynamic nature of oxygen levels in cell culture. By using Fick's law, a per-cell oxygen consumption rate was calculated. The current sensor provided a facile method to integrate oxygen measurement with common phase-contrast and fluorescence microscopy techniques.

In the follow up study (Chapter 4), the sensor was incorporated into HepG2 cultures to examine the changes of oxygen levels. In these cultures, oxygen levels decreased drastically and HepG2 cells were exposed to hypoxic conditions within 24 hrs; even for low seeding densities. A per-cell oxygen consumption rate calculation revealed that HepG2 cells consume approximate 30 times more oxygen (29 fmol/min/cell) than other cells types such as NIH 3T3 confirming their high metabolic characteristics. In high density cultures, oxygen flux (a measure of oxygen consumption rate) measurements showed an asymptotic behavior reaching the theoretical maximum of the culture. By reducing the diffusive barrier for oxygen to travel (reducing the medium height), the oxygen fluxes increased demonstrating that the cells were oxygen starved at these densities. Unlike monolayer cultures, HepG2 cells attach to their neighboring cells to form cell clusters. Due to their high consumption rate, oxygen gradients were measured across these clusters with the middle showing the lowest oxygen levels. The ability to provide such a detailed spatial resolution could be potentially useful for other cell types that form cell aggregates such as cancer cells and stem cells.

In the final study (Chapter 5), we demonstrated the application of the oxygen sensor in microfluidic systems to generate physiologically relevant oxygen levels for cell culture purposes. The non-invasive, emission detection method of the current sensor was perfectly suited for microfluidic technologies. In addition, the PDMS shell of the sensor provided a facile way to be integrated into any PDMS based devices without further modifications. To regulate the oxygen levels on-chip, water with controlled dissolved oxygen concentration was used instead of gases. This was achieved through the development of an off-chip gas exchanger. Oxygen regulation using liquid mitigated against pervaporation effects associated with using gas control and provided a way to regulate the oxygen levels on-chip without exposing cells to shear stress. Physiologically relevant oxygen levels (P_{O2} = 0.03 atm to 0.05 atm) and oxygen gradients were easily achieved with the current device. The oxygen sensor provided real-time oxygen measurements and the results were confirmed with finite element simulations.

6.2 Recommendations for Future Work

The studies completed in this dissertation provide the foundation for facile integration of oxygen measurements into a variety of different cell lines. In addition, this sensor formulation could be easily tailored for different cell culture formats. Moreover, new applications for oxygen measurements could provide a useful tool to assess cell health and functions. As such, we present two potential projects as part of the future works.

6.2.1 Bead-Based Oxygen Sensors

The sensors developed in this dissertation have a planar geometry that were tailored for 2-dimensional cell culture formats where oxygen measurements were made directly beneath regions of cell attachment. For 3-dimensional (3D) cell cultures where cells are distributed within a scaffold or gel of extra-cellular matrix, new sensor formats are required in order to examine the distributions of oxygen levels across 3D space. Bead-based oxygen sensors could be potentially applicable since it can be easily distributed along with the cells into 3D formats. As such, we have begun to develop bead-based oxygen sensors using a microfluidic system. The sensor was prepared by incorporating the phosphorescent dye PtTFPP into PDMS beads. The resulting sensor showed oxygen-dependent quenching effects similar to the planar sensors (Figure 6.2).

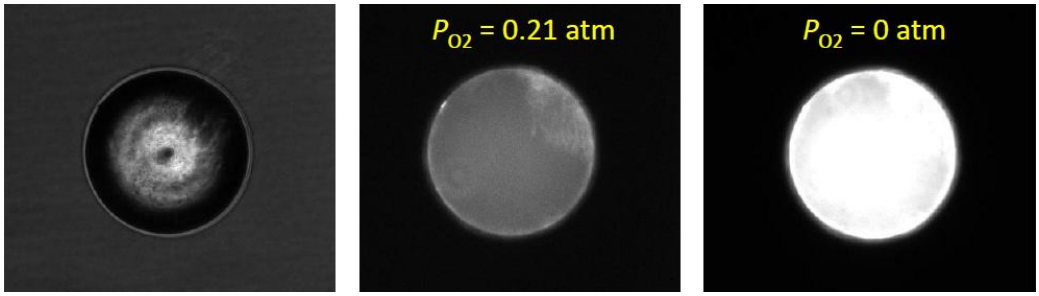

Figure 6.2 Bead-based oxygen sensors. Phase contrast of the sensor (a) and fluorescence images of the sensor under P_{O2} = 0.21 atm (b) and P_{O2} = 0 atm (c).

6.2.2 Oxygen Measurements for Drug Toxicity Assay

In Chapter 4, we successfully demonstrated the ability to culture HepG2 cells and quantify their oxygen consumption rate. While hepatocyte cultures (primary and

immortalized cell lines) have been routinely used for drug toxicity studies, however, oxygen consumption rate from these cells has not been directly used to quantify cellular toxicity response. We propose that oxygen measurements in hepatocyte cutlures could provide additional information regarding cell response to drug toxicity. Changes in oxygen consumption could provide more sensitive information regarding drug response compared to past assays. In addition, other fluorescence-based assays (Live/Dead Cell Viability Assay; MTT Assasy) could be used simultaneously as a comparison.

References

[1] Witkowski, J. A. “Carrel,Alexis and the Mysticism of Tissue-Culture.” *Med. Hist.* **1979**, *23*, 279-296.

[2] Witkowski, J. A. “Experimental Pathology and the Origins of Tissue-Culture - Loeb,Leo Contribution.” *Med. Hist.* **1983**, *27*, 269-288.

[3] Semenza, G. L. “Life with oxygen.” *Science* **2007**, *318*, 62-64.

[4] Harvey Lodish, A. B., Parul Matsudaira, Chris A. Kaiser, Kreiger M, Scott MP, Zipursky SL, Darnell J *Molecular Cell Biology*, 5th Edition ed.; W.H. Freeman and Company, 2004.

[5] Ward, J. P. T. “Oxygen sensors in context.” *Biochim. Biophys. Acta-Bioenerg.* **2008**, *1777*, 1-14.

[6] Aragones, J.; Fraisl, P.; Baes, M.; Carmeliet, P. “Oxygen Sensors at the Crossroad of Metabolism.” *Cell Metab.* **2009**, *9*, 11-22.

[7] Brahimi-Horn, M. C.; Pouyssegur, J. “Oxygen, a source of life and stress.” *FEBS Lett.* **2007**, *581*, 3582-3591.

[8] Brezis, M.; Rosen, S.; Silva, P.; Epstein, F. H. “Renal Ischemia - a New Perspective.” *Kidney Int.* **1984**, *26*, 375-383.

[9] Chow, D. C.; Wenning, L. A.; Miller, W. M.; Papoutsakis, E. T. “Modeling pO(2) distributions in the bone marrow hematopoietic compartment. I. Krogh's model.” *Biophys. J.* **2001**, *81*, 675-684.

[10] Csete, M. Oxygen in the cultivation of stem cells. In *Stem Cell Biology: Development and Plasticity*, 2005; Vol. 1049; pp 1-8.

[11] Herman, B. *Fluorescence Microscopy*; Bios Scientific Pub Ltd, 1998.

[12] Lakowicz, J. R. *Principles of Fluorescence Sepctroscopy*; Plenum Press: New York, 1983.

[13] Chandel, N. S.; Budinger, G. R. S. “The cellular basis for diverse responses to oxygen.” *Free Radic. Biol. Med.* **2007**, *42*, 165-174.

[14] Papkovsky, D. B.; O'Riordan, T. C. “Emerging applications of phosphorescent metalloporphyrins.” *J. Fluoresc.* **2005**, *15*, 569-584.

[15] Merkel, T. C.; Bondar, V. I.; Nagai, K.; Freeman, B. D.; Pinnau, I. "Gas sorption, diffusion, and permeation in poly(dimethylsiloxane)." *J. Polym. Sci. Pt. B-Polym. Phys.* **2000**, *38*, 415-434.

[16] Basu, S.; Khan, A. L.; Cano-Odena, A.; Liu, C. Q.; Vankelecom, I. F. J. "Membrane-based technologies for biogas separations." *Chem. Soc. Rev.*, *39*, 750-768.

[17] Singh, A.; Freeman, B. D.; Pinnau, I. "Pure and mixed gas acetone/nitrogen permeation properties of polydimethylsiloxane [PDMS]." *J. Polym. Sci. Pt. B-Polym. Phys.* **1998**, *36*, 289-301.

[18] Haibing Zhang, A. C. "The Permeability Characteristics of Silicone Rubber"; SAMPE Fall Technical Conference, 2006, Dallas, TX.

[19] Park, T. H.; Shuler, M. L. "Integration of cell culture and microfabrication technology." *Biotechnol. Prog.* **2003**, *19*, 243-253.

[20] Alentiev, A. Y.; Shantarovich, V. P.; Merkel, T. C.; Bondar, V. I.; Freeman, B. D.; Yampolskii, Y. P. "Gas and vapor sorption, permeation, and diffusion in glassy amorphous teflon AF1600." *Macromolecules* **2002**, *35*, 9513-9522.

[21] Stern, O.; Volmer, M. "The fading time of fluorescence." **1919**, *20*, 183-188.

[22] Bacon, J. R.; Demas, J. N. "Determination of Oxygen Concentrations by Luminescence Quenching of a Polymer-Immobilized Transition-Metal Complex." *Anal. Chem.* **1987**, *59*, 2780-2785.

[23] Carraway, E. R.; Demas, J. N.; Degraff, B. A.; Bacon, J. R. "Photophysics and Photochemistry of Oxygen Sensors Based on Luminescent Transition-Metal Complexes." *Anal. Chem.* **1991**, *63*, 337-342.

[24] Peterson, J. I.; Fitzgerald, R. V.; Buckhold, D. K. "Fiber-Optic Probe for Invivo Measurement of Oxygen Partial-Pressure." *Anal. Chem.* **1984**, *56*, 62-67.

[25] Foster, B. *Optimizing Light Microscopy for Biological and Clinical Laboratories*; Kendall/Hunt Publishing Company: Dubuque, 1997.

[26] Atkuri, K. R.; Herzenberg, L. A.; Niemi, A. K.; Cowan, T.; Herzenberg, L. A. "Importance of culturing primary lymphocytes at physiological oxygen levels." *Proc. Natl. Acad. Sci. U. S. A.* **2007**, *104*, 4547-4552.

[27] Allen, J. W.; Bhatia, S. N. "Formation of steady-state oxygen gradients in vitro - Application to liver zonation." *Biotechnol. Bioeng.* **2003**, *82*, 253-262.

[28] Allen, J. W.; Khetani, S. R.; Bhatia, S. N. "In vitro zonation and toxicity in a hepatocyte bioreactor." *Toxicol. Sci.* **2005**, *84*, 110-119.

[29] Sitkovsky, M.; Lukashev, D. "Regulation of immune cells by local. tissue oxygen tension: Hif1 alpha and adenosine receptors." *Nat. Rev. Immunol.* **2005**, *5*, 712-721.

[30] Malda, J.; Klein, T. J.; Upton, Z. "The roles of hypoxia in the In vitro engineering of tissues." *Tissue Eng.* **2007**, *13*, 2153-2162.

[31] Higgins, J. M.; Eddington, D. T.; Bhatia, S. N.; Mahadevan, L. "Sickle cell vasoocclusion and rescue in a microfluidic device." *Proc. Natl. Acad. Sci. U. S. A.* **2007**, *104*, 20496-20500.

[32] Brown, J. M.; William, W. R. "Exploiting tumour hypoxia in cancer treatment." *Nat. Rev. Cancer* **2004**, *4*, 437-447.

[33] Ezashi, T.; Das, P.; Roberts, R. M. "Low O-2 tensions and the prevention of differentiation of hES cells." *Proc. Natl. Acad. Sci. U. S. A.* **2005**, *102*, 4783-4788.

[34] Lennon, D. P.; Edmison, J. M.; Caplan, A. I. "Cultivation of rat marrow-derived mesenchymal stem cells in reduced oxygen tension: Effects on in vitro and in vivo osteochondrogenesis." *J. Cell. Physiol.* **2001**, *187*, 345-355.

[35] Sahaf, B.; Atkuri, K.; Heydari, K.; Malipatlolla, M.; Rappaport, J.; Regulier, E.; Herzenberg, L. A.; Herzenberg, L. A. "Culturing of human peripheral blood cells reveals unsuspected lymphocyte responses relevant to HIV disease." *Proc. Natl. Acad. Sci. U. S. A.* **2008**, *105*, 5111-5116.

[36] Mamchaoui, K.; Saumon, G. "A method for measuring the oxygen consumption of intact cell monolayers." *Am. J. Physiol.-Lung Cell. Mol. Physiol.* **2000**, *278*, L858-L863.

[37] Tokuda, Y.; Crane, S.; Yamaguchi, Y.; Zhou, L.; Falanga, V. "The levels and kinetics of oxygen tension detectable at the surface of human dermal fibroblast cultures." *J. Cell. Physiol.* **2000**, *182*, 414-420.

[38] Kuang, Y. N.; Walt, D. R. "Detecting oxygen consumption in the proximity of Saccharomyces cerevisiae cells using self-assembled fluorescent nanosensors." *Biotechnol. Bioeng.* **2007**, *96*, 318-325.

[39] Guarino, R. D.; Dike, L. E.; Haq, T. A.; Rowley, J. A.; Pitner, J. B.; Timmins, M. R. "Method for determining oxygen consumption rates of static cultures from microplate measurements of pericellular dissolved oxygen concentration." *Biotechnol. Bioeng.* **2004**, *86*, 775-787.

[40] Wang, W. J.; Upshaw, L.; Strong, D. M.; Robertson, R. P.; Reems, J. A. "Increased oxygen consumption rates in response to high glucose detected by a novel oxygen biosensor system in non-human primate and human islets." *J. Endocrinol.* **2005**, *185*, 445-455.

[41] O'Donovan, C.; Hynes, J.; Yashunski, D.; Papkovsky, D. B. "Phosphorescent oxygen-sensitive materials for biological applications." *J. Mater. Chem.* **2005**, *15*, 2946-2951.

[42] Puklin, E.; Carlson, B.; Gouin, S.; Costin, C.; Green, E.; Ponomarev, S.; Tanji, H.; Gouterman, M. "Ideality of pressure-sensitive paint. I. Platinum tetra(pentafluorophenyl)porphine in fluoroacrylic polymer." *J. Appl. Polym. Sci.* **2000**, *77*, 2795-2804.

[43] Lee, S. K.; Okura, I. "Photostable optical oxygen sensing material: Platinum tetrakis(pentafluorophenyl)porphyrin immobilized in polystyrene." *Anal. Commun.* **1997**, *34*, 185-188.

[44] Bukowski, R. M.; Ciriminna, R.; Pagliaro, M.; Bright, F. V. "High-performance quenchometric oxygen sensors based on fluorinated xerogels doped with [Ru(dpp)(3)](2+)." **2005**, *77*, 2670-2672.

[45] Bukowski, R. M.; Davenport, M. D.; Titus, A. H.; Bright, F. V. "O-2-responsive chemical sensors based on hybrid xerogels that contain fluorinated precursors." **2006**, *60*, 951-957.

[46] Bedlek-Anslow, J. M.; Hubner, J. P.; Carroll, B. F.; Schanze, K. S. "Micro-heterogeneous oxygen response in luminescence sensor films." *Langmuir* **2000**, *16*, 9137-9141.

[47] Pinnau, I.; Toy, L. G. "Gas and vapor transport properties of amorphous perfluorinated copolymer membranes based on 2,2-bistrifluoromethyl-4,5-difluoro-1,3-dioxole/tetrafluoroethylene." *J. Membr. Sci.* **1996**, *109*, 125-133.

[48] Geankoplis, C. J. *Transport Process and Unit Operations*, 3rd ed.; Prentice-Hall Inc: Englewood Cliffs, NJ, 1993.

[49] Khalil, G. E.; Chang, A.; Gouterman, M.; Callis, J. B.; Dalton, L. R.; Turro, N. J.; Jockusch, S. "Oxygen pressure measurement using singlet oxygen emission." *Rev. Sci. Instrum.* **2005**, *76*, 054101-1 - 8.

[50] Murphy, B.; Kirwan, P.; McLoughlin, P. "Study of the impact of penetrant characteristics upon diffusion into Teflon membranes to further assess the performance of an ATR/FTIR sensor." *Anal. Bioanal. Chem.* **2003**, *377*, 195-202.

[51] Ballet, F. “Hepatotoxicity in drug development: Detection, significance and solutions.” **1997**, *26*, 26-36.

[52] Kaplowitz, N. “Idiosyncratic drug hepatotoxicity.” *Nat. Rev. Drug Discov.* **2005**, *4*, 489-499.

[53] DiMasi, J. A.; Hansen, R. W.; Grabowski, H. G. “The price of innovation: new estimates of drug development costs.” *J. Health Econ.* **2003**, *22*, 151-185.

[54] Khetani, S. R.; Bhatia, S. N. “Microscale culture of human liver cells for drug development.” **2008**, *26*, 120-126.

[55] Balis UJ, B. K., Dwarakanath B, Bhatia SN, Sullivan SJ, Yarmush ML, Toner M. “Oxygen Consumption Characteristics of Porcine Hepatocytes.” *Metab Eng* **1999**, 49-62.

[56] Kietzmann, T.; Jungermann, K. “Modulation by oxygen of zonal gene expression in liver studied in primary rat hepatocyte cultures.” *Cell Biol. Toxicol.* **1997**, *13*, 243-255.

[57] Camp, J. P.; Capitano, A. T. “Induction of zone-like liver function gradients in HepG2 cells by varying culture medium height.” *Biotechnol. Prog.* **2007**, *23*, 1485-1491.

[58] Rotem, A.; Toner, M.; Bhatia, S.; Foy, B. D.; Tompkins, R. G.; Yarmush, M. L. “Oxygen Is a Factor Determining in-Vitro Tissue Assembly - Effects on Attachment and Spreading of Hepatocytes.” **1994**, *43*, 654-660.

[59] Kidambi, S.; Yarmush, R. S.; Novik, E.; Chao, P.; Yarmush, M. L.; Nahmias, Y. “Oxygen-mediated enhancement of primary hepatocyte metabolism, functional polarization, gene expression, and drug clearance.” *Proc. Natl. Acad. Sci. U. S. A.* **2009**, *106*, 15714-15719.

[60] Nishikawaa, M.; Kojimaa, N.; Komoria, K.; Yamamoto, T.; Fujii, T.; Sakai, Y. “Enhanced maintenance and functions of rat hepatocytes induced by combination of on-site oxygenation and coculture with fibroblasts.” *J. Biotechnol.* **2008**, *133*, 253-260.

[61] Zhdanov, A. V.; Ogurtsov, V. I.; Taylor, C. T.; Papkovsky, D. B. “Monitoring of cell oxygenation and responses to metabolic stimulation by intracellular oxygen sensing technique.” *Integr. Biol.* **2010**, *2*, 443-451.

[62] Thomas, P. C.; Halter, M.; Tona, A.; Raghavan, S. R.; Plant, A. L.; Forry, S. P. “A Noninvasive Thin Film Sensor for Monitoring Oxygen Tension during in Vitro Cell Culture.” *Anal. Chem.* **2009**, *81*, 9239-9246.

[63] Schofield, C. J.; Ratcliffe, P. J. “Oxygen sensing by HIF hydroxylases.” *Nat. Rev. Mol. Cell Biol.* **2004**, *5*, 343-354.

[64] Carmeliet, P.; Dor, Y.; Herbert, J. M.; Fukumura, D.; Brusselmans, K.; Dewerchin, M.; Neeman, M.; Bono, F.; Abramovitch, R.; Maxwell, P.; Koch, C. J.; Ratcliffe, P.; Moons, L.; Jain, R. K.; Collen, D.; Keshet, E. “Role of HIF-1 alpha or in hypoxia-mediated apoptosis, cell proliferation and tumour angiogenesis.” *Nature* **1998**, *394*, 485-490.

[65] Piret, J. P.; Lecocq, C.; Toffoli, S.; Ninane, N.; Raes, M.; Michiels, C. “Hypoxia and CoCl2 protect HepG2 cells against serum deprivation- and t-BHP-induced apoptosis: a possible anti-apoptotic role for HIF-1.” *Exp. Cell Res.* **2004**, *295*, 340-349.

[66] Wang, G. L.; Semenza, G. L. “General Involvement of Hypoxia-Inducible Factor-I in Transcriptional Response to Hypoxia.” *Proc. Natl. Acad. Sci. U. S. A.* **1993**, *90*, 4304-4308.

[67] Parrinello, S.; Samper, E.; Krtolica, A.; Goldstein, J.; Melov, S.; Campisi, J. “Oxygen sensitivity severely limits the replicative lifespan of murine fibroblasts.” *Nat. Cell Biol.* **2003**, *5*, 741-747.

[68] Keith, B.; Simon, M. C. “Hypoxia-inducible factors, stem cells, and cancer.” *Cell* **2007**, *129*, 465-472.

[69] Simon, M. C.; Keith, B. “The role of oxygen availability in embryonic development and stem cell function.” *Nat. Rev. Mol. Cell Biol.* **2008**, *9*, 285-296.

[70] Jungermann, K.; Kietzmann, T. “Oxygen: Modulator of metabolic zonation and disease of the liver.” *Hepatology* **2000**, *31*, 255-260.

[71] Carmeliet, P.; Jain, R. K. “Angiogenesis in cancer and other diseases.” *Nature* **2000**, *407*, 249-257.

[72] Hagen, T.; Taylor, C. T.; Lam, F.; Moncada, S. “Redistribution of intracellular oxygen in hypoxia by nitric oxide: Effect on HIF1 alpha.” *Science* **2003**, *302*, 1975-1978.

[73] Yun, Z.; Maecker, H. L.; Johnson, R. S.; Giaccia, A. J. “Inhibition of PPAR gamma 2 gene expression by the HIF-1-regulated gene DEC1/Stra13: A mechanism for regulation of adipogenesis by hypoxia.” *Dev. Cell* **2002**, *2*, 331-341.

[74] Wright, W. E.; Shay, J. W. “Inexpensive low-oxygen incubators.” *Nat. Protoc.* **2006**, *1*, 2088-2090.

[75] Vollmer, A. P.; Probstein, R. F.; Gilbert, R.; Thorsen, T. "Development of an integrated microfluidic platform for dynamic oxygen sensing and delivery in a flowing medium." *Lab Chip* **2005**, *5*, 1059-1066.

[76] Park, J.; Bansal, T.; Pinelis, M.; Maharbiz, M. M. "A microsystem for sensing and patterning oxidative microgradients during cell culture." *Lab Chip* **2006**, *6*, 611-622.

[77] Lam, R. H. W.; Kim, M. C.; Thorsen, T. "Culturing Aerobic and Anaerobic Bacteria and Mammalian Cells with a Microfluidic Differential Oxygenator." *Anal. Chem.* **2009**, *81*, 5918-5924.

[78] Polinkovsky, M.; Gutierrez, E.; Levchenko, A.; Groisman, A. "Fine temporal control of the medium gas content and acidity and on-chip generation of series of oxygen concentrations for cell cultures." *Lab Chip* **2009**, *9*, 1073-1084.

[79] Adler, M.; Polinkovsky, M.; Gutierrez, E.; Groisman, A. "Generation of oxygen gradients with arbitrary shapes in a microfluidic device." *Lab Chip* **2010**, *10*, 388-391.

[80] Heo, Y. S.; Cabrera, L. M.; Song, J. W.; Futai, N.; Tung, Y. C.; Smith, G. D.; Takayama, S. "Characterization and resolution of evaporation-mediated osmolality shifts that constrain microfluidic cell culture in poly(dimethylsiloxane) devices." *Anal. Chem.* **2007**, *79*, 1126-1134.

[81] Unger, M. A.; Chou, H. P.; Thorsen, T.; Scherer, A.; Quake, S. R. "Monolithic microfabricated valves and pumps by multilayer soft lithography." *Science* **2000**, *288*, 113-116.

[82] Song, J. W.; Gu, W.; Futai, N.; Warner, K. A.; Nor, J. E.; Takayama, S. "Computer-controlled microcirculatory support system for endothelial cell culture and shearing." *Anal. Chem.* **2005**, *77*, 3993-3999.